Solid-state sensors for trace hydrogen gas detection

Constantinos Christofides and Andreas Mandelis
Photoacoustic and Photothermal Sciences Laboratory, Department of Mechanical Engineering, and Center for Hydrogen and Electrochemical Studies (CHES), University of Toronto, Toronto, Ontario M5S 1A4, Canada

(Received 27 November 1989; accepted for publication 14 May 1990)

This paper reviews the development, history, theoretical basis, and experimental performance of solid-state hydrogen detectors under flow-through conditions available to date such as pyroelectric, piezoelectric, fiber optic, and electrochemical devices. Semiconductor hydrogen detectors will only be reviewed briefly, as excellent reviews on this subject already exist. In view of the fact that almost all the devices that will be discussed later in this paper use Pd as a hydrogen trap, we devote a subsection to examining the role of palladium as a catalyst as well as some of the characteristics of the Pd-H_2 system. Non-solid-state hydrogen sensors, such as the flame ionization detector are not the object of this review. A useful feature of this review is a comparison of operating characteristics of each device in a general table in Sec. VII. In that section a general discussion is presented, including a critical comparison of the capabilities and parameters of various solid-state hydrogen sensors in the form of a table showing data collected from the literature. The Pd-fiber optic sensor is the most sensitive optical device operating at room temperature. The Pd-photopyroelectric sensor appears to be most economical and second best in sensitivity at room temperature; it has the best potential for high signal-to-noise operation at the widest temperature range, down to cryogenic temperatures. The Pd-field effect transistor devices exhibit the second highest sensitivity at elevated temperatures.

TABLE OF CONTENTS

List of acronyms

List of symbols

I. Introduction

I. A. Why hydrogen sensors?

I. B. The role of palladium as catalyst

II. Pyroelectric sensors

II. A. dc-Pyroelectric chip (Pd-$LiTaO_3$)

II. B. ac-Photopyroelectric thin film (Pd-PVDF-PPE) sensor

III. Piezoelectric sensors

III. A. Piezoelectric quartz crystal microbalance (PQCMB)

III. B. Surface acoustic wave (SAW) detectors

IV. Fiber optic sensors (FOS)

V. Electrochemical (HUP) hydrogen sensors

VI. Semiconductor hydrogen flow-through sensors

VII. General discussion, comparisons, and concluding remarks

Acknowledgments

References

LIST OF ACRONYMS

EMF:	Potential difference
FET:	Field effect transistor
FOS:	Fiber optic sensors
IDT:	Interdigital transducer
IGFET:	Insulated gate field effect transistor
HUP:	Hydrogen uranyl phosphate
MIS:	Metal insulator semiconductor
MOS:	Metal oxide semiconductor
MOSFET:	Metal oxide semiconductor field effect transistor
P-C:	Pressure-concentration
PD:	Photodiode
PGA:	Pyroelectric gas analyzer
ppb:	Part per billion
PPE:	Photopyroelectric
ppm:	Part per million
PQCMB:	Piezoelectric quartz crystal microbalance
PVDF:	Polyvinylidene fluoride
SAW:	Surface acoustic wave
STP:	Standard temperature and pressure
UHV:	Ultrahigh vacuum

LIST OF SYMBOLS

A:	Capacitor surface
A_H:	Constant depends of the rates of the hydrogen reaction
A_0:	Total coated area of the PQCMB

 0021-8979/90/1800R1-30$03.00

A_I: Absorbance
A_r: Temperature constant
A_s: Surface of the SAW coated layer
C: Capacitance ($= C_p + C_a$)
C_0: Concentration
c_1, d_1: Rate constants of hydrogen dissociation
C_A, C_B: Volume specific heat
C_a: Input capacitance of the preamplifier
c_e, c_i: Rate constants of the hydrogen reaction
C_p: Pyroelectric capacitance
C_v: Volume heat capacity
D_T: Thermal diffusivity of the pyroelectric detector
d_e, d_i: Rate constants of the hydrogen reaction
dQ: Charge density
E_{A_L}, E_{B_L}: Illuminated areas
$E_{A_{el}}, E_{B_{el}}$: Electrode areas
E_x: Experimental constant
f: Modulation frequency
F: Resonance frequency of the PQCMB and SAW detector
F_a: Faraday
$f(R_0)$: Kubelka–Munk function
g: Geometrical factor
H: Heat flux
I: Transmitted light intensity
I_0: Incident light intensity
k: Thermal conductivity
$K(T)$: Temperature constant
k_c: Constant related to the resonant frequency of the PQCMB
k_1, k_2: Material constant for SAW substrate
$K_{1,2}$: PPE system constants
K_n: Positive integer
L: Palladium thickness (SAW)
$L_{s,R}$: Inductances
l_s: Propagation path in thin coating (SAW)
l_R: Reference propagation path
M_{Pd}: Mass of the chemically sensitive palladiuim layer
M_{PG}: Mass of the piezoelectric crystal
M_0: Molecular weight
m_a: Molar absorptivity
n: Concentrations of the absorbed hydrogen atoms (i: interface, b: bulk, and e: surface)
N: Number of absorption sites (i: interface, b:bulk, and e: surface)
NA: Numerical aperture of the fiber optic
N_A: Avogadro number
N_F: Frequency constant (PQCMB)
N_{H_s}: Saturated number of the adsorbed and absorbed atoms/ions
n_0: Refractive index of the air
n_1: Refractive index of the core of FOS
n_2: Refractive index of the cladding of FOS
P_g: Partial pressure of the gas
P_{H_2}: Molecular hydrogen partial pressure
$P^C_{H_2}$: Hydrogen partial pressure at 1 atm
P_{lim}: Lowest pressure sensitivity
p: Pyroelectric coefficient
$p_{A,B}$: Pyroelectric coefficients of the two PPE detectors
P_{11}, P_{44}: Pockels' coefficients
R: Universal gas constant
R_A: Resistance of the preamplifier input
R_0: Reflectance of a semi-infinite medium
R_p: Resistance of the pyroelectric capacitor
R_s: Response time of the hydrogen detector
R_T: Total resistance
S_c: Scattering coefficient
T: Absolute temperature
T_0: Initial temperature
t: Time
Q: Charge density on a pyroelectric capacitor
U: Acoustic velocity
$U_{s,R}$: Acoustic velocity in the coated and noncoated layer, respectively
u, w: Constants dependent on the palladium thickness
V: Potential
V_c: Volume of the test cell
$V_{Pd,R}$: Signal obtained by the Pd-NiCr and uncoated reference electrodes respectively
$V_{S,R}$: Voltages output through inductances L_S and L_R (SAW device)
V_G: Gate voltages (FET device)
V_M: Maximum output voltage
W_A, W_B: Incident optical fluxes
W_r: Flow rate
z: Thickness of the quartz crystal microbalance
z_0: Transducer thickness (pyroelectric crystal and film)
α: Absorption coefficient
δH: Extra heat flux (Pd-$LiTaO_3$ device)
$\delta\xi$: Measured response signal (piezoelectric, pyroelectric...)
$\delta\xi_{max}$: Maximum measured response signal of the hydrogen sensors
$\delta\xi_{min}$: Minimum measured response signal of the hydrogen sensors
δS_{max}: Maximum measured photopyroelectric response
δS_{min}: Minimum measured photopyroelectric response
ΔC_0: Concentration of the absorbed gas molecules
ΔE: Potential measured across the electrolyte
ΔE_a: Heat of adsorption
ΔE_{cell}: Potential measured across the electrochemical cell
$\Delta H_{Pd,R}$: Net heat flux in the two electrodes Pd-NiCr and Reference-NiCr, respectively
ΔF: Frequency shift of the PQCMB and SAW device
ΔF_{PQCMB}: Frequency shift of the PQCMB
ΔF_{SAW}: Frequency shift of the SAW device
ΔM: Mass of the absorbed gas molecules
ΔS: Normalized differential output signal of PPE sensor
ΔU: Shift of the acoustic velocity
ΔV_{max}: Maximum voltage output
ΔV_s: Saturated voltage difference
Δz: Thickness of the Pd layer coated on the quartz

	crystal microbalance
$\Delta\Phi$:	Shift of the phase delay of SAW sensor
$\Delta\phi$:	Phase shift due to the optical path length
ϵ:	Permittivity constant of vacuum
η:	Surface emissivity
Θ_{is}:	Surface coverage saturation
$\Theta_{i,b,e}$:	Coverage (i:interface, b:bulk, and e:surface)
$\Theta_{\min}$:	Minimum coverage
λ,μ:	Lamé constants
ρ:	Piezoelectric film density
σ:	$=(\lambda+\mu)/(\lambda+2\mu)$
τ:	Characteristic circuit time constant
τ_{th}:	Thermal time constant
Φ:	Phase delay of SAW sensor
ϕ:	Optical path length (FOS)
Φ_E:	Electric phase shift (FOS)
Φ_F:	Quantum yield of fluorescence
Φ_0:	Flux of the surface impinging molecules
$\Psi_{i,c}$:	Reflected and critical angles

I. INTRODUCTION

A. Why hydrogen sensor?

Today's modern industrialized society has brought to the world a number of goods and services, as well as a series of problems related to technological development. The ever increasing industrialization makes it absolutely necessary to constantly monitor and control air pollution in the environment, in factories, laboratories, hospitals, and generally technical installations.

In recent years, hydrogen has grown to be one of the most useful gases. In fact, in many industries such as chemical, food, metallurgical, electronic, and others, hydrogen is increasingly taking the role of a raw material.[1] Some examples of the importance of detecting hydrogen gas are as follows: (a) H_2 is absorbed by several metals causing the precipitation of hydrides in titanium and zirconium and, in the case of steel, hydrogen embrittlement. (b) The majority of pipework in a chemical plant is encased in insulation in order to prevent heat loss; however, if water penetrates, induced corrosion occurs undetected. (c) During electroplating, hydrogen is often evolved and this enters the metal substrate. Since the "oil crisis" of 1973 hydrogen gas has attracted public attention as a clean energy resource, because of its high heat capacity. One of the reasons for which hydrogen may play an important energetic role in the near future, is the fact that this gas presents some hopes for the world to avoid a mean global warming of at least 2 °C by the mid 21st century due to the greenhouse effect. Furthermore, it is because of its anticipated usefulness that hydrogen is expected to play a role of increasing importance primarily as an intermediary in the manufacture of synthetic fuels.[2] Research and development work in advanced on-board fuel is of foremost importance for the transportation industry. Specialists believe that hydrogen-fueled motor vehicles will soon be a reality.[3] However, the increasing use of hydrogen gas should not be considered as one without disadvantages. In fact, a number of problems arise involving storage of this gas. A hydrogen leak in large quantities should be avoided because hydrogen when mixed with air in the ratio of 4.65–93.9 vol % is explosive.[4] For this reason, among others, it has become very important to develop highly sensitive hydrogen detectors to prevent accidents due to H_2 gas leakage, thus saving lives and equipment. Such detectors should allow continuous monitoring of the concentration of gases in the environment in a quantitative and selective way. The following list gives both constraints and requirements for an "ideal" chemical detector: (i) Chemically selective, (ii) reversible, (iii) fast, (iv) highly sensitive, (v) durable, and (vi) noncontaminating and nonpoisoning; other constraints involve requirements for (vii) simple operation, (viii) small size (portability), (ix) simple fabrication, (x) relative temperature insensitivity, and (xi) low noise. In addition, this control system should be financially accessible to potential users. Another area in which hydrogen gas detectors are also very useful is the field of surface science. In fact, devices which operate on the principle of a decrease of the work function of Pd by adsorption of H_2 are the main means for the study of the surface-gas interaction in the Pd-H_2 system.

This paper reviews the development, history, theoretical basis, and experimental performance of solid-state hydrogen detectors under flow-through conditions available to date such as pyroelectric, piezoelectric, fiber optic, and electrochemical devices. Semiconductor hydrogen detectors will only be reviewed briefly, as excellent reviews on this subject already exist. Non-solid-state hydrogen sensors, such as the flame ionization detector are not the object of this review.[5] A useful feature of this review is a comparison of operating characteristics of each device in a general Table in Sec. VII. In view of the fact that almost all the devices that will be discussed later in this paper use Pd as a hydrogen trap, we devote the next subsection to examining the role of palladium as a catalyst as well as some of the characteristics of the Pd-H_2 system.

B. The role of palladium as a catalyst

Catalytic effects play an important role in the field of gas detection. Solid-state gas sensors are directly related to the phenomenon of catalysis. Catalytic processes not only control the rate at which a chemical reaction approaches equilibrium (this affects considerably the response time in the case of gas detection), but also affect selectivity.

It is well known that Pd has high hydrogen solubility.[6] The absorption of hydrogen by Pd during electrolysis was observed in 1868 by Thomas Grahab.[6] Since then, the palladium-hydrogen system has been studied extensively. Because of its selectivity to hydrogen absorption, Pd has been employed as a filter for hydrogen purification, and it has also been used to provide hydrogen selectivity for various hydrogen detectors.[6] The absorption of hydrogen in Pd depends on temperature and hydrogen concentration. Figure 1 shows a schematic comparison of solubility of hydrogen in Ni, Pd, and Pt metals at a pressure of 1 atm as a function of temperature.[6] A comparison between Pd and Pt as gates in metal

oxide semiconductor (MOS) devices has also been made by Armgarth *et al.*[7] These authors have shown that Pd is superior as gate material for the detection of small amounts of hydrogen at room temperature. They also showed that Pt is more suitable for high hydrogen concentrations. From Fig. 1 one can easily see that Pd is predominant in hydrogen-sensor technology due to the much higher solubility of hydrogen in Pd than in Ni or Pt. In order to discuss a hydrogen-detector response as a function of concentration (or hydrogen partial pressure), it is necessary to recall the surface-gas interaction in the hydrogen-palladium system. Gas-surface interactions are important as energy transfer mechanisms at the gas-solid interface on an atomic scale; so is the adsorption-absorption-desorption process.

The various experimental results discussed in this review paper concerning H_2 detection have usually been interpreted as a function of the hydrogen concentration (or hydrogen partial pressure). In the hydrogen-palladium system the flux of the surface impinging molecules, Φ_0, of a particular gas is proportional to the partial pressure of the gas, P_g, the gas molecular weight, M_0, and the absolute temperature, T, assuming low enough concentrations and no interference from other ambient gases. According to the kinetic theory of gases the flux of gas molecules is given by Eq. (1):[8,9]

$$\Phi_0\left(\frac{\text{molecules}}{\text{cm}^2\,\text{s}}\right)=\frac{N_A P_g}{\sqrt{2\pi M_0 RT}}\approx 3\times 10^{22}\frac{P_g(\text{Pa})}{\sqrt{M_0 T}}, \quad (1)$$

where N_A is the Avogadro number and R is the universal gas constant.

The majority of investigators in the field of the hydrogen sensors interpreted their results as a function of a controlled known experimental parameter, such as the molecular hydrogen partial pressure P_{H_2}. For this purpose the atomic hydrogen pressure in the trapping medium must be given as a function of molecular pressure in the gas phase. The adsorbed hydrogen gas molecules are dissociated on the catalytic metal surface (usually Pd), and the H atoms are absorbed into the Pd bulk. Some of these absorbed atoms diffuse to the metal-substrate interface. According to Lundström,[10] equilibrium exists between the number of adsorbed H on the surface and that at the back interface. In the case of an inert atmosphere (such as N_2 or Ar) the only reaction taking place on the metal surface is[10,11]

$$H_2 \underset{d_1}{\overset{c_1}{\rightleftarrows}} 2H_a. \quad (2)$$

This reaction represents the dissociation of hydrogen on the Pd catalyst. H_a is the adsorbed hydrogen atom and c_1 and d_1 are the rate constants of the reaction. After the absorption of hydrogen into, and diffusion through, the Pd film, another reaction takes place:[10]

$$H_a \underset{c_e}{\overset{d_e}{\rightleftarrows}} H_b \underset{c_i}{\overset{d_i}{\rightleftarrows}} H_{ai}, \quad (3)$$

where c_e, c_i, d_e, and d_i are rate constants; H_b and H_{ai} are the atomic hydrogen concentrations in the bulk and at the back interface, respectively. Assuming that the number of hydrogen absorption sites per unit area on the Pd surface is N_e, and that on the Pd-substrate interface is N_i, one can write[10]

$$\frac{n_i}{N_i-n_i}=\frac{d_i}{c_i}\frac{n_b}{N_b-n_b}=\frac{c_e d_i}{d_e c_i}\frac{n_e}{N_e-n_e}, \quad (4)$$

where N_b is the number of absorption sites in the bulk (per unit volume $\times$ thickness) of the Pd film. n_i, n_b, and n_e are the concentrations of the adsorbed hydrogen atoms on the Pd-substrate interface, bulk, and surface, respectively. At equilibrium the forward and backward rates are equal so that

$$c_1[H_2]=d_1[H_a]^2. \quad (5)$$

Furthermore, from Eqs. (2), (4), and (5)[10]

$$\frac{n_e}{N_e-n_e}=\sqrt{\frac{c_1}{d_1}P_{H_2}}. \quad (6)$$

One can note that the partial hydrogen pressure, P_{H_2}, has been introduced in Eq. (6), a fact which leads to a more direct interpretation of a number of experimental results, which are expressed as a function of hydrogen partial pressure. Thus, it is necessary to introduce the *coverage* of hydrogen at the surface $\Theta_e = n_e/N_e$, and at the Pd-substrate interface, $\Theta_i = n_i/N_i$. By combining Eqs. (4) and (6) and by taking into account the definition of the coverage one can write

$$\frac{\Theta_i}{1-\Theta_i}=A_H\frac{\Theta_e}{1-\Theta_e}=K\sqrt{P_{H_2}}, \quad (7)$$

where

$A_H \equiv c_e d_i/d_e c_i$ and K is a constant ($K\equiv\sqrt{c_1/d_1}$)[10] which depends mainly on the difference in absorption energies at the surface and interface, respectively. K is given by the relation[8]

$$K(T)=2.5\times 10^{-5}\sqrt{\frac{A_r}{TM_o}}\times\exp\left(-\frac{\Delta E_a}{2RT}\right)\ [\text{Pa}^{-1/2}], \quad (8)$$

where A_r is a temperature constant (given in units of gK) and ΔE_a is the heat of adsorption "per molecule," i.e., per

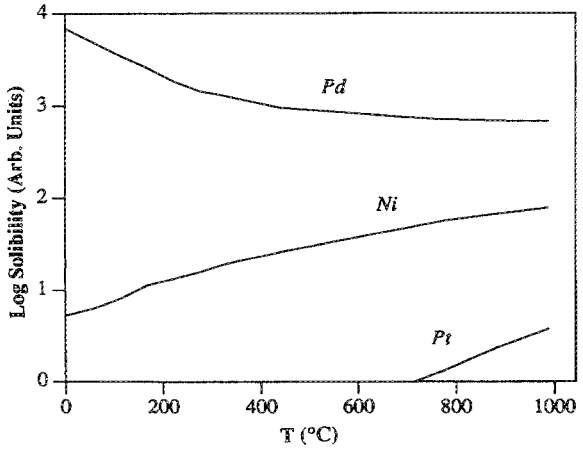

FIG. 1. Schematic comparison of solubility of hydrogen in Pd, Ni, and Pt at a pressure of 1 atm as a function of temperature (from Ref. 6).

two atoms, if the adsorption is dissociative such as in the case of the Pd-H_2 system. The value of ΔE_a is approximately 1 eV.[10,12] Finally the coverage of hydrogen, Θ_i, can be written as a function of the hydrogen partial pressure, P_{H_2}:[8,9,13]

$$\Theta_i = \frac{K(T)\sqrt{P_{H_2}}}{1 + K(T)\sqrt{P_{H_2}}}. \tag{9}$$

According to Lundström[10] a linear relationship may be assumed between the measured response signals $\delta\xi$ (which can be voltage, pyroelectric signal, frequency shift, optical signal, etc.) and the coverage of hydrogen atoms, Θ_i, under the condition $P_{H_2} < 200$ Pa:

$$\delta\xi = \delta\xi_{\max}\Theta_i , \tag{10}$$

where $\delta\xi_{\max}$ is the maximum signal response of the hydrogen detector corresponding to complete surface coverage saturation, and $\Theta_i = \Theta_{is}$ at the saturation regime (i.e., $t \to \infty$). Then, Eq. (10) may be written

$$\delta\xi_s = \delta\xi_{\max}\Theta_{is} . \tag{11}$$

Using Eqs. (10) and (11), it is easy to rewrite Eq. (11) in the form of the Langmuir isotherm in the saturation regime:

$$\delta\xi_s = \delta\xi_{\max}\left(\frac{K(T)\sqrt{P_{H_2}}}{1 + K(T)\sqrt{P_{H_2}}}\right). \tag{12}$$

Equation (12) is valid only in the case where the palladium layer is clean (not oxidized) and exposed to pure hydrogen.[9]

II. PYROELECTRIC SENSORS

A. Introduction and historical perspective

The phenomenon of pyroelectricity is not new. It was observed almost three hundred years ago. Measurements of the pyroelectric effect first appeared shortly before World War I.[14] Several theoretical and experimental studies of the pyroelectric effect have been performed during the last twenty years. Pyroelectricity is the manifestation of the spontaneous polarization dependence on temperature of certain anisotropic solids. This effect is exhibited only by solids which satisfy crystallographic requirements such as: (i) the crystal lattice must have no center of symmetry and (ii) the crystal must have no more than one axis of rotational symmetry. A pyroelectric material becomes electrically neutral, when in a constant temperature environment for a period of time. If there is a small change of the temperature, ΔT, the pyroelectric material becomes electrically polarized and a voltage arises between certain directions in the material. This unique property of pyroelectric materials led to many applications during the last few years. The pyroelectric thermometer,[15] the pyroelectric anemometers,[16–19] the radiation monitor,[20] and the pyroelectric infrared image sensors[21] may be counted among others.

In 1981, Zemel *et al.*[22] reported the first pyroelectric chemical sensor (Pd-$LiTaO_3$). Except for three more publications reported by Amico *et al.*,[23] by Zemel,[24] and by Amico and Zemel,[25] all in 1985, the pyroelectric phenomenon did not appear to generate interest in the chemical detector field, thus the pyroelectric chemical detector was not further developed. Very recently an experimental effort of the present authors led to the development of a promising new, simple, sensitive, fast, and purely photopyroelectric chemical detector based on polyvinylidene fluoride (PVDF): The ac Pd-PVDF photopyroelectric sensor for H_2 gas detection.[26–30]

This section describes the operating characteristics of the dc and ac pyroelectric hydrogen sensors. The two detectors were coated with palladium electrodes which are well known for their ability to selectively adsorb hydrogen. Exposure to hydrogen gas was shown to produce a signal difference between the Pd and reference electrodes of both dc and ac pyroelectric detectors. This was tentatively attributed to thermal energy transfer as a result of the adsorption and dissociation of hydrogen molecules on the Pd surface. The fundamental difference between the operating mechanisms of the dc and ac pyroelectric sensors is the fact that for the dc detector the shift on the Pd-$LiTaO_3$ pyroelectric signal is due to the change of temperature resulting from the deposition of adsorption energy,[24] while for the ac sensor a shift on the Pd-PVDF pyroelectric coefficient appears to be the operating principle, presumably due to electrostatic interactions at the Pd-PVDF interface.[26,27] A comparison of ac and dc devices will be presented with respect to their sensitivity, chemical selectivity, and stability.

B. Theoretical background

Pyroelectric materials exhibit the property that the polarization vector is a function of temperature. As the temperature varies, the surface charge also varies due to dimensional changes in the pyroelectric. This property results in a potential difference between the two opposite surfaces of the material, generally known as pyroelectricity. According to Zemel, the charge density, Q, on a pyroelectric capacitor could be written in the following form:[24]

$$Q = -C_p(V - V_0) + p(T)(\langle T\rangle - T_0) , \tag{13}$$

where $V - V_0$ is the potential drop across the pyroelectric capacitor, C_p is the capacitance, p is the pyroelectric coefficient, and T is the temperature. T_0 is the initial temperature. $\langle T\rangle$ is the instantaneous temperature rise of the pyroelectric averaged over its thickness. Therefore, the total pyroelectric current will be the integral of the current density over the capacitor surface, A. Using Eq. (13) one can write

$$I = \int_A \frac{dQ}{dt}\,dA = \int_A \left(-C_p A\frac{dV}{dt} + p\frac{d\langle T\rangle}{dt}\right) dA . \tag{14}$$

The output measured voltage under load conditions may be written as[24]

$$V(t) = \frac{pA\exp(-t/\tau)}{C}\int_0^t \exp(t'/\tau)\left\langle\frac{\delta T}{\delta t'}\right\rangle dt' , \tag{15}$$

where t is time, $C = C_p + C_a$ with C_p being the pyroelectric capacitance, and C_a the input capacitance of the preamplifier; τ is a characteristic circuit time constant $\tau = RC$; $R_T = [(1/R_p) + (1/R_A)]^{-1}$ where R_p and R_A are the resistance of the pyroelectric capacitor and of the preamplifier input, respectively. If the temperature varies sinusoidally at frequency f, the pyroelectric voltage will be

$$V(f) = \frac{2\pi jfpR_T A\langle T\rangle}{1 + 2\pi jf\tau}, \tag{16}$$

where $j^2 = -1$.

The temperature distribution across the pyroelectric transducer (z direction) may be estimated using the Fourier heat conduction equation:[24]

$$\frac{\partial T}{\partial t} = D_T \frac{\partial^2 T}{\partial z^2}, \tag{17}$$

where D_T is the thermal diffusivity of the pyroelectric detector, defined as the ratio of the thermal conductivity k to the volume heat capacity C_v. Thus, it is easy to show that

$$\left\langle \frac{\partial T}{\partial t} \right\rangle = \frac{k}{C_v} \left\langle \frac{\partial^2 T}{\partial z^2} \right\rangle = \frac{1}{C_v z_0} \Delta H(t), \tag{18}$$

where $\Delta H(t) = H(0,t) - H(z_0,t)$ is the net heat flux into the pyroelectric transducer of thickness z_0. Substituting Eq. (18) into Eq. (15) leads to:

$$V(t) = \frac{pA \exp(-t/\tau)}{CC_v z_0} \int_0^t \Delta H(t') \exp(t'/\tau) dt'. \tag{19}$$

Evaluating the pyroelectric response at $t = \tau_{th}$, where τ_{th} is a thermal time constant, which is long compared to the RC time constant τ of the pyroelectric, Eq. (19) becomes

$$V(t) = (pR_T A / C_v z_0) \Delta H(t). \tag{20}$$

In Table I some typical experimental parameters can be found for the ac and dc devices in the second and third column, respectively. In the following discussion we will use Eq. (20) as the above condition is satisfied in the case of available experimental work.

C. dc-pyroelectric chip (Pd-$LiTaO_3$)

1. Experimental apparatus

A schematic diagram of a dc-pyroelectric gas analyzer (dc-PGA) is shown in Fig. 2(a). The dc-PGA is made of Z-cut, single-crystal $LiTaO_3$ wafers, typically 230 μm thick. The device fabrication steps are basically the same as those used in semiconductor device photolithography. The electrodes (NiCr) are fabricated photolithographically. One of the NiCr surfaces has been coated with a catalyst material (Pd in this case). A heater was integrated in the pyroelectric device in order to control the temperature-time profile $T(t)$. The differential voltage, ΔV, of PGA is directly proportional to the net heat flux into the pyroelectric device and is given by the relation

$$\Delta V = V_{Pd} - V_R, \tag{21}$$

where V_{Pd} is the signal obtained by the Pd-NiCr electrode, and V_R is the signal obtained by the uncoated reference electrode. A heater was incorporated into the pyroelectric $LiTaO_3$ layer [Fig. 2(b)]. The transducer thus absorbed the thermal energy produced by the heater and gave rise to two different electrical voltages: V_{Pd} and V_R. From Eqs. (20) and (21) the differential output signal may be written as[24]

$$\Delta V = (pAR_T/C_v z_0)(\Delta H_{Pd} - \Delta H_R), \tag{22}$$

where ΔH_{Pd} and ΔH_R are two net heat fluxes in the two electrodes Pd-NiCr and Reference-NiCr, respectively. Since the heat flow in both pyroelectric materials from the heater is the same [see Fig. 2(b)], the differential voltage is zero. As the reference electrode contains no chemically sensitive catalyst, its heat loss is the reference state for the measurements. On the other hand, any additional heat gain or loss,

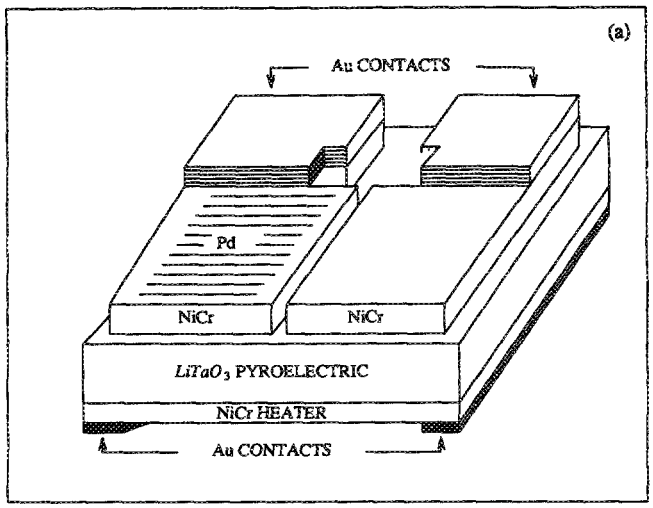

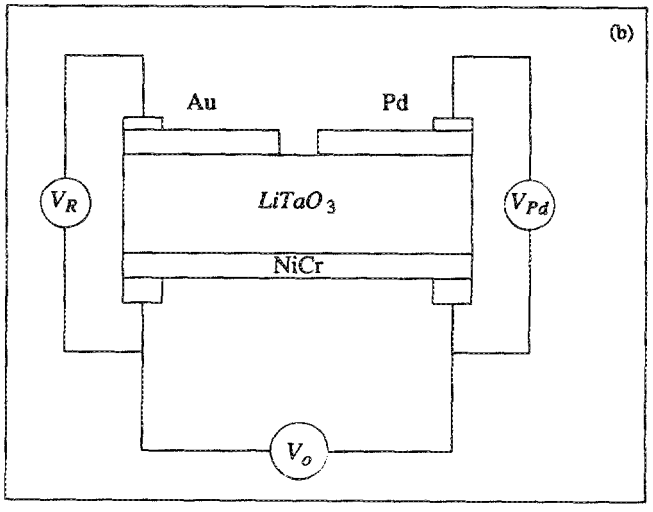

FIG. 2. (a) Schematic of the dc-pyroelectric detector showing details of construction. (b) Side view of the dc-pyroelectric detector (from Ref. 24).

TABLE I. Some experimental parameters useful for dc and ac pyroelectric hydrogen detectors.

Experimental parameters	Pd-PPE[a]	Pd-$LiTaO_3$[b]
Pyroelectric sensor thickness, z_0 (cm)	2.8×10^{-3}	23×10^{-3}
Amplifier input resistance at 20 Hz, R_A (Ω)	10^8	10^9
Amplifier input capacitance, C_A (pF)	16	20
Pd thickness, L (cm)	2.85×10^{-6}	30×10^{-6}?
Pd total Area, A (cm^2)	0.1	0.1

[a] From Ref. 27.
[b] From Ref. 24.

depends on the exothermicity or not of the chemical reaction. The sign of the differential ΔV response will be an indication of the kind of interaction associated with the chemical processes on the catalyst. The introduction of hydrogen into the test cell, and the absorption of the gas by Pd, causes an extra heat δH in the Pd-NiCr electrode and thus the differential voltage is

$$\delta V = (ApR_T/z_0C_v)\delta H . \quad (23)$$

The adsorption and desorption of hydrogen, due to changes in its partial pressure in the cell environment, generates δH and thus a temperature gradient between the two electrodes.

2. Results and discussion

The dc-PGA was exposed to a mixture of 1% hydrogen in nitrogen flowing at atmospheric pressure over the device at a rate of 180 ml/min. Typical experimental results are shown in Figs. 3(a)–3(c). Figures 3(a) and (b) show the variation of the reference signal V_R and the Pd-NiCr signal V_{Pd} as a function of time. In these figures, one can note the influence of the introduction (and cut off) of O_2, N_2, and H_2 on the Pd-PGA through the variation of V_R and V_{Pd} signals. According to Zemel, the negative portion arises from the cooling of the dc-pyroelectric detector after the reactions have reached saturation.[24] Figure 3(c) shows the temperature profile of the Pd-PGA. We note that the temperature varies only upon introduction of hydrogen. From Fig. 3(c) one can conclude that the smaller signals (after O_2, N_2-on and -off) are due to the adiabatic heating and cooling when valves are opened or closed during the gas cycles.[24] Figure 4 shows the variation of the differential PGA signal δV as a function of time [Data collected from Figs. 3(a) and 3(b)]. The above preliminary results are only qualitative; unfortunately no new results have been reported concerning this pyroelectric device.

Besides its multilayer fabrication complexity, this dc pyroelectric sensor has proved to be extremely susceptible to temperature fluctuations due to environmental factors (e.g., valve opening and closing during gas cycles). An additional disadvantage of this (otherwise quite sensitive) sensor may be the long delay for gas detection due to diffusive transport of thermal energy from the Pd electrode region to the reference (Au) electrode. These factors appear to have limited the development of purely pyroelectric devices as gas sensors to date.

The next subsection describes the novel and simple thin-film photopyroelectric[26–30] solid-state sensor for the detection of minute concentrations of hydrogen gas. The PPE device is expected to solve many problems encountered with the purely pyroelectric, and perhaps other, gas detectors, with the added element of fabrication simplicity. The experimental characteristics of the PGA device will be compared to those of the photopyroelectric sensor.

D. ac-photopyroelectric thin film (Pd-PVDF-PPE) detector

1. Experimental apparatus

An overview of the experimental arrangement of the photopyroelectric sensor is described in Fig. 5(a). The instrumentation consisted of an RCA laser diode powered by an ac current supply. The output laser beam, 4 mW *p-t-p* multimode at $\pm$ 800 nm, was directed to a three-way fiber-optic coupler where it was split at approximately 16%, 34%, and 50%. Detailed schematics of the PVDF cells, active, "*A*," and reference, "*B*," as well as the feedback control are shown in Fig. 5(b). As is shown in that figure the 16% inten-

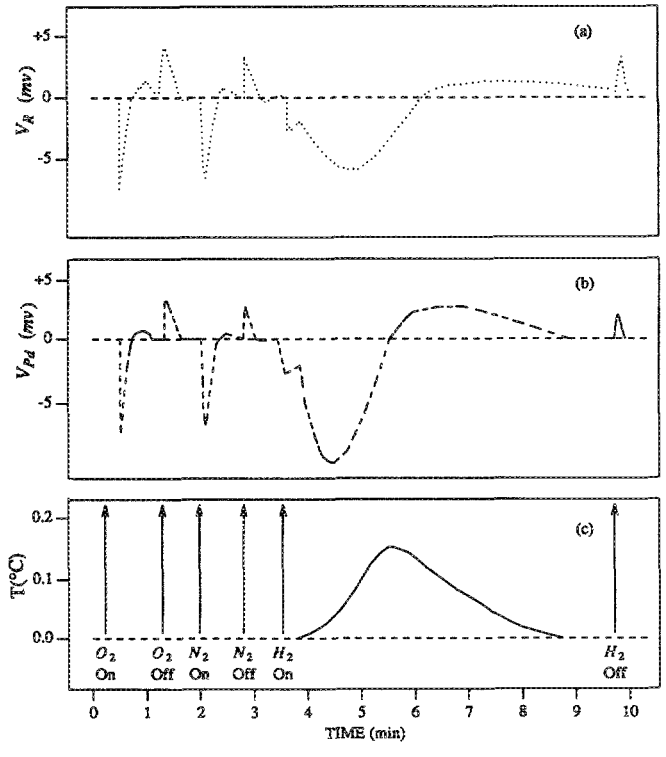

FIG. 3. Individual component responses of the dc-PGA to the admission of various gases in the measurement chamber; (a) the Pd electrode, (b) the gold electrode, and (c) the temperature profile (from Ref. 24).

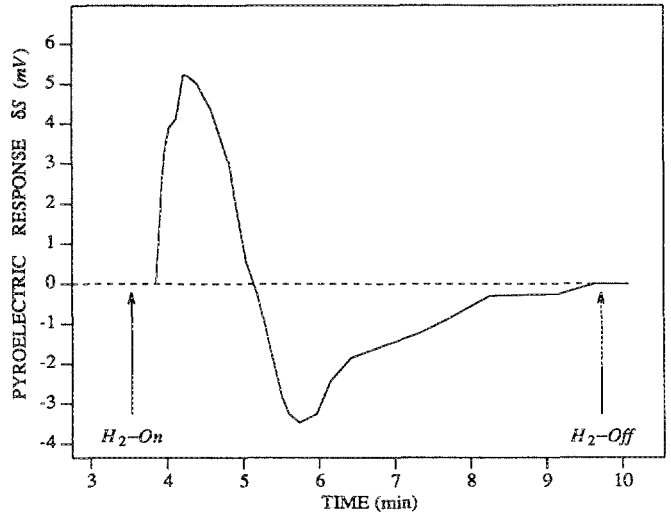

FIG. 4. PGA pyroelectric response as a function of time ($[H_2] = 1\%$). [Data collected from Figs.3(a) and 3(b).]

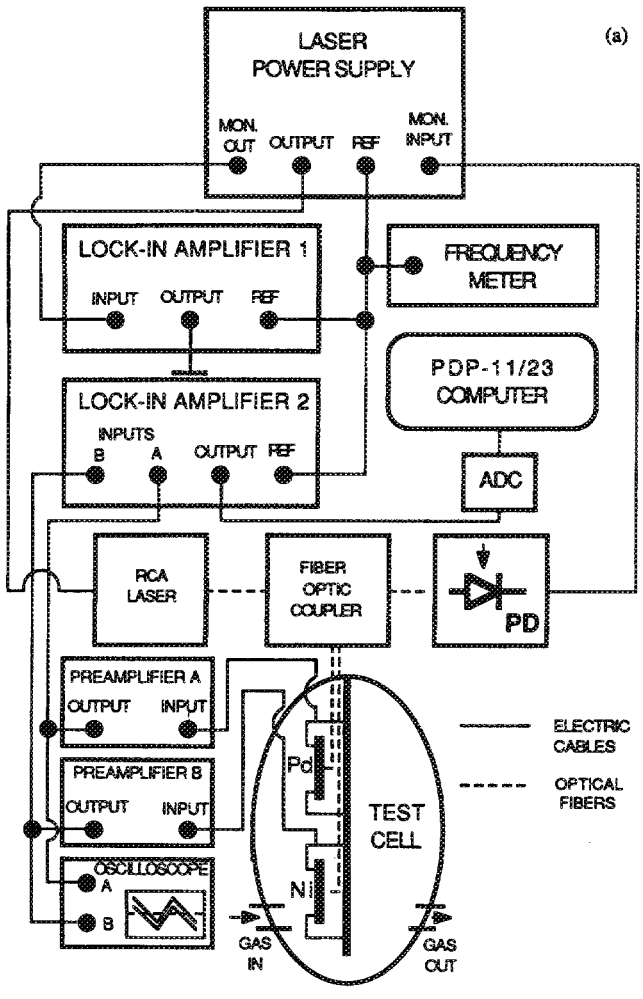

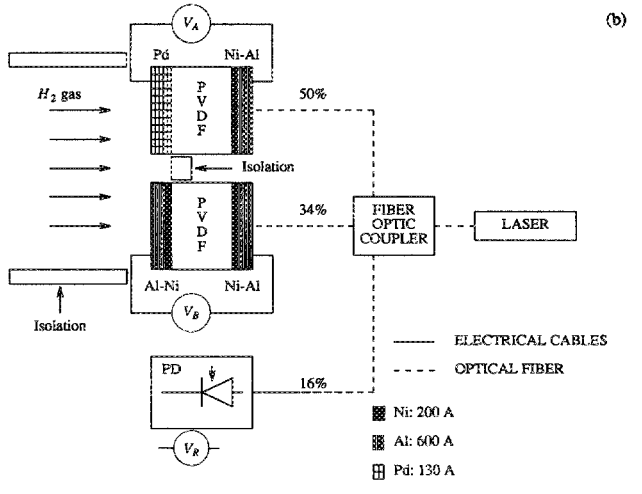

FIG. 5. (a) Schematic overview of the photopyroelectric sensor set-up. (b) Detail of the gas flow chamber, including the active Pd-coated and reference Al-Ni-coated PVDF cells (from Refs. 25–27).

sity fiber optic channel was directed to a photodiode (PD), the output of which was then sent to the "monitor" input of the homemade laser current supply for preamplification and feedback control of the laser current, as well as for synchronous lock-in detection. The feedback control consisted of using this reference signal to correct temporal intensity variations in the modulated laser beam. In the same figure information is given concerning the thicknesses of different coatings. Before discussing the photopyroelectric response upon introduction of hydrogen, it is important to note that the gas contacted the Pd and Al-Ni surfaces only [see Fig. 5(b)] while the surfaces subjected to IR irradiation were isolated from the exposed gases. The ac photopyroelectric detector differential signals from two 28-μm-thick PVDF films, were bandpass filtered and preamplified by two low-noise preamplifiers. On one PVDF film a thickness of 285-Å-Pd had been evaporated (henceforth designated "unit A"), and the other PVDF film was first covered with 200 Å standard Ni and then with 600 Å of Al ("unit B"), The lock-in amplifiers were referenced by the ac laser current supply. The output of lock-in 1 was connected to lock-in amplifier 2, which was equipped with a ratio option, allowing the absolute value of the normalized differential function output:[31]

$$|\Delta S| = \frac{|V_A - V_B|}{|V_R|}, \tag{24}$$

where V_A is the signal obtained from the Pd – PVDF electrode, V_B is the signal generated by the Al-Ni-PVDF electrode, and V_R is the ac laser power reference output obtained from the photodiode PD. The two pyroelectric transducers absorbed the thermal energy of the infrared beams and thus gave rise to two different electrical voltages, V_A and V_B.

2. Analysis of the photopyroelectric response

In these experiments, harmonic modulation of the absorbed beam intensity resulted in harmonic changes in ΔT which subsequently gave rise to synchronous ac voltages $V_A(f)$ and $V_B(f)$:[26,28,29]

$$V_A(f) = \frac{\eta p_A W_A(f) E_{A_l}}{\epsilon C_A E_{A_{el}}}, \tag{25.1}$$

$$V_B(f) = \frac{\eta p_B W_B(f) E_{B_l}}{\epsilon C_B E_{B_{el}}}, \tag{25.2}$$

where the subscripts "A" and "B" refer to the active (Pd) and the reference electrode (Al–Ni), respectively; p_A and p_B are the pyroelectric coefficients; W_A and W_B are the incident optical fluxes; C_A and C_B are volume-specific heats; η is the illuminated surface emissivity; ϵ is the PVDF dielectric constant; E_{A_l} and E_{B_l} are the illuminated areas; and $E_{A_{el}}$ and $E_{B_{el}}$ are the electrode areas ($E_{A_l} < E_{A_{el}}$ and $E_{B_l} < E_{B_{el}}$). The surface emissivity η is in fact a nonradiative efficiency factor, indicating the percent of conversion of optical energy to thermal energy. η in our case is very high due to the high absorptance of the Ni-Al metallized PVDF in the infrared region of the spectrum. ϵ is the permittivity constant of vacuum (see Table II). From Eqs. (24), (25.1), and (25.2) the output differential signal prior to the introduction of hydrogen gas in the test cell generated in the Pd-PVDF and the Al-Ni-PVDF electrodes may be shown to be[26–30]

TABLE II. Some properties of PVDF pyroelectric film. From Ref. 32.

Properties of PVDF	
Dielectric permittivity, ϵ(F/cm)	1.06×10^{-12}
Relative permittivity, ϵ/ϵ_0	12
Capacitance, C_p (pF)	37.9
Pyroelectric coefficient (at 20 °C), p_e (C/cm^2K)	3×10^{-9}
Volume resistivity (Ω cm)	1.5×10^{15}
Density (gr/cm^3)	1.78
Thermal diffusivity D_t (cm^2/s)	5.2×10^{-4}
Thermal time constant τ_{th} (s)	5

$$\Delta S(f)=\frac{1}{V_R}\frac{\eta}{\epsilon C}\left(\frac{p_A W_A(f)E_{A_L}}{E_{A_{el}}}-\frac{p_B W_A(f)E_{B_L}}{E_{B_{el}}}\right), \tag{26}$$

where $f\approx20$ Hz and $C_A=C_B\equiv C$, due to the impermeability of the PVDF film bulk by hydrogen. The lock-in output channels were connected to a computer, through the ports of an A/D converter, for data storage and analysis of the ratioed output signal amplitude, ΔS. In Eq. (26) the absolute value signs have been replaced by brackets, because it was found that the active electrode signal V_A increased in the presence of H_2, while V_B remained unaltered.

Since the heat flows into the PPE devices from the laser beams are not equal [$W_A\neq W_B$; see Fig. 5(b)], the two photopyroelectric voltages were different. Thus, the magnitude of ΔS was minimized in the beginning of each experiment by a judicious choice of gain on the preamplifiers, prior to introduction of the gas into the test cell ($V_B\approx V_A\rightarrow|V_B-V_A|\rightarrow\Delta S\approx0$). As a result of the above considerations we can write that, initially,

$$\frac{p_A[\mathrm{O}]W_A E_{A_L}}{E_{A_{el}}}=\frac{p_B[\mathrm{O}]W_B E_{B_L}}{E_{B_{el}}}, \tag{27.1}$$

where the bracketed quantities signify ambient H_2 concentration. The introduction of hydrogen into the test cell does not change the heat fluxes because $\Delta T(f)$ is solely determined by the infrared laser beams. Thus in the following discussion we will assume that $W\equiv W_A=W_B$ because of the choice of gain on the preamplifiers. It is also clear that during the measurements, the distances of the optical fibers from the PVDF illuminated surface remain constant, and because of that we can also assume that the two areas are equal: $E_L\equiv E_{A_L}=E_{B_L}$. The relation (27.1), which is imposed because $\Delta S=0$, may then be rewritten as

$$\frac{p_A[\mathrm{O}]}{E_{A_{el}}}=\frac{p_B[\mathrm{O}]}{E_{B_{el}}}. \tag{27.2}$$

Upon introduction of hydrogen in the test cell a rise of the normalized differential voltage was caused by the H_2 (atomic or molecular) adsorption on, and absorption in, the palladium film. This normalized differential voltage is given by the relation:

$$\delta S(f)=\frac{1}{V_R}\frac{\eta W(f)E_L}{\epsilon C}\left[\left(\frac{p_A[\mathrm{H}]}{E_{A_{el}}}\right)-\left(\frac{p_B[H]}{E_{B_{el}}}\right)\right]. \tag{28}$$

In the absence of H_2([H] = 0), all the coefficients (pyroelectric coefficients, electrodes and illuminated areas, and volume-specific heats) of the two terms in Eq. (28) can be assumed identical. With the introduction of hydrogen in the chamber, if there is an increase of δS, Eqs. (26)–(28) lead to a new relationship between the pyroelectric factors,

$$\frac{p_A[\mathrm{H}]}{E_{A_{el}}}>\frac{p_B[\mathrm{H}]}{E_{B_{el}}}. \tag{29}$$

From the above inequality one can conclude that the introduction of hydrogen in the test cell gives rise to a photopyroelectric response because of the change of the pyroelectric coefficient and/or the change of the effective palladium electrode area (change in the PVDF capacitance). In order to identify the most probable mechanism generating the hydrogen response both possibilities have been examined separately.

Hypothesis 1: Response due to the change of the pyroelectric coefficients.

We assume that $E_{el}\equiv E_{A_{el}}=E_{B_{el}}$. Before the introduction of the hydrogen ([H] = 0) the pyroelectric coefficients of the Pd and Ni-Al coated PVDF films may be assumed identical: $p_A[\mathrm{O}]=p_B[\mathrm{O}]$. Thus, for an interaction of H_2 gas with the Pd to cause an excess differential voltage δS, after hypothesis 1, Eq. (28) may be written as:[26–28]

$$\delta S=K_1(p_A[\mathrm{H}]-p_B[\mathrm{H}]), \tag{30.1}$$

where $K_1(\equiv\eta WE_L/\epsilon CE_{el}V_R)$ is a system constant. However, $p_B[\mathrm{H}]=p_B[\mathrm{O}]\approx p_A[\mathrm{O}]$, and this is due to the lack of response of the Al-Ni surface to H_2 gas. This shows that in the absence of hydrogen gas $\delta S=0$. With the above considerations and writing $\Delta p_A\equiv p_A[\mathrm{H}]-p_A[\mathrm{O}]$, Eq. (30.1) may be modified:

$$\delta S(f)=K_1\Delta p_A. \tag{30.2}$$

For small departures from the $p_A[\mathrm{O}]$ value, the derivative of the pyroelectric coefficient p_A with respect to the density of absorbed atoms (or ions), N_H, gives the Δp_A variation:[26–28]

$$\Delta p_A=\left(\frac{\partial p_A}{\partial N_H}\right)_{N_{H_0}}N_H. \tag{30.3}$$

In Eq. (30.3) $(\partial p_A/\partial N_H)_{N_{H_0}}$ is a measurable material constant of the Pd-metallized PVDF. Using Eqs. (30.2) and (30.3), in the saturation regime (i.e., $t\rightarrow\infty:\delta S\rightarrow\delta S_s$) we can write

$$\delta S_s=K_1\left(\frac{\partial p_A}{\partial N_H}\right)_{N_{H_0}}N_{H_s}, \tag{30.4}$$

where N_{H_s} is the saturated number of the adsorbed and absorbed hydrogen atoms/ions.

Hypothesis 2: Response due to change in the effective electrical area.

We assume that: $p\equiv p_A=p_B$. Before the introduction of hydrogen, the areas of the two electrodes of the Pd- and Ni-Al-coated PVDF films may also be assumed identical:

$E_{A_{el}}[O] = E_{B_{el}}[O]$. Thus, for interaction of H_2 gas with Pd to cause an excess differential voltage δS, according to hypothesis 2, Eq. (28) may be written as

$$\delta S = K_2\left(\frac{1}{E_{A_{el}}[H]} - \frac{1}{E_{B_{el}}[H]}\right), \tag{31.1}$$

where $K_2(\equiv \eta W p E_L/\epsilon C V_R)$ is a system constant. However, $E_{B_{el}}[H] = E_{B_{el}}[O] \approx E_{A_{el}}[O]$, and this is due to the null response of the Al-Ni surface to H_2 gas. This shows that in the absence of hydrogen gas $\delta S = 0$. With the above considerations, writing $\Delta E_{A_{el}} = E_{A_{el}}[H] - E_{A_{el}}[O]$, and for small departures from the $E_{A_{el}}[O]$ value, Eq. (31.1) may be written[26]

$$\delta S(f) \approx -K_2 \frac{\Delta E_{A_{el}}}{(E_{A_{el}}[O])^2}. \tag{31.2}$$

Under these conditions, the derivative of the electrode area $E_{A_{el}}$ with respect to N_H, is the $\Delta E_{A_{el}}$ variation:

$$\Delta E_{A_{el}} = \left(\frac{\partial \Delta E_{A_{el}}}{\partial N_H}\right)_{N_{H-0}} N_H = \left(\frac{\partial E_{A_{el}}[H]}{\partial N_H}\right)_{N_{H-0}} N_H. \tag{31.3}$$

Using Eqs. (31.2) and (31.3), in the saturation regime

$$\delta S_s = -K_2 \frac{1}{(E_{A_{el}}[O])^2}\left(\frac{\partial E_{A_{el}}[H]}{\partial N_H}\right)_{N_{H-0}} N_{H_s}. \tag{31.4}$$

The likelihood of either hypothesis 1 or 2 being the major mechanism responsible for the PPE sensor signal δS in the presence of H_2 was further examined. Toward this goal two PVDF films were coated with 285 Å Pd on oppositely polarized surfaces. These films were used as detectors. It has been shown that the positively polarized electrode gives an induced normalized voltage which increases as a function of time.[26] The voltage from the negatively polarized electrode has been found to decrease as a function of time in a manner essentially symmetric with respect to the equilibrium level (prior to the exposure to hydrogen). This experiment shows that the pyroelectric response is sensitive to the *sign* of the charges at the PVDF surface next to the Pd layer. The results are consistent with the presence of charged H^+ ions (Fig. 6) at the Pd-PVDF interface.[26] In the case of the positively polarized electrode, the additional positive charges (protons) will raise the electrostatic potential of the front surface with respect to the unexposed back surface. This would result in an increased photopyroelectric voltage, as observed. On the contrary, absorbed protons are expected to neutralize (cancel) the field due to the negative charges at the surface of the negatively polarized electrode, thus lowering the electrostatic potential of the front surface. This would result in the observed decreased PPE voltage. After several "test" experiments concerning the polarization of the films, at this time it appears[26,29] that the most likely operating mechanism involves an electrostatic interaction of the absorbed proton field on the metallic side of the interface with the molecular dipole field in the electret, thus affecting the average dipole moment and the total polarization, P. Therefore, the prevalent model (Hypothesis 1) leads to the prediction of a shift of the pyroelectric coefficient, p_{Pd}, with the Pd-absorbed proton density, N_H:

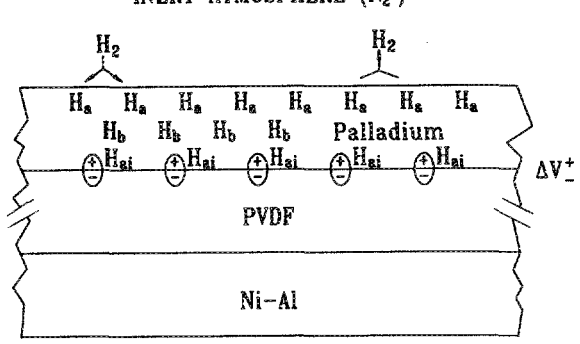

FIG. 6. Schematic picture showing chemical reactions on the Pd surface, hydrogen transport to the bulk and to the Pd-PVDF interface.

$$\frac{\partial p_{Pd}}{\partial N_H} = \frac{\partial}{\partial T}\left(\frac{\partial P}{\partial N_H}\right). \tag{32}$$

3. Experimental results

Typical experimental results for various hydrogen concentrations are shown in Figs. 7(a) and 7(b). This figure shows photopyroelectric responses as a function of time.[25–27] These experiments have been performed under the same conditions ($T = 20$ °C, flow rate: 500 ml/min) using Pd coating of two different thicknesses. At the times indicated by the H_2-On markers, the sample gas was allowed through the test cell. After saturation [horizontal part of the $\delta S(t)$ curves; t is the time] and at times indicated by the H_2-Off markers, pure nitrogen flowed continuously through the cell in order to remove the absorbed hydrogen. As a result, δS decreased to the baseline existing prior to the introduction of the sample gas. Figure 8 shows the variation of δS_s as a function of hydrogen concentration in the range of 40–2000 ppm.

Figure 9 shows the variation of R_s as a function of H_2 flow rates (500–60 ml/min), $T = 20$ °C, and H_2 concentration $= 5\%$ in nitrogen. The flow rate was found not to influence δS_s significantly. The flow rate does, however, influence the response time of the sensor, which increases monotonically (3–10 min) with decreasing flow rate between 500 ml/min and 60 ml/min. The experimental results show that the photopyroelectric sensor is completely reversible and durable.[26,27]

The PPE hydrogen sensor analysis concerns very low partial pressures (< 2000 ppm). Thus, a Langmuirian approach has been used for the phenomenological interpretation of the sensor response, similar to earlier analyses of the Pd-MOS hydrogen detector.[10,33,34] The general equation of the Langmuir isotherm adapted to the photopyroelectric experimental condition is[27]

$$\delta S_s \approx \delta S_{max}\left(\frac{K(T)\sqrt{P_{H_2}}}{1 + K(T)\sqrt{P_{H_2}}}\right), \tag{33}$$

where δS_{max} is the maximum signal response of the photopyroelectric detector corresponding to complete surface coverage saturation. Figure 8 (solid curve) shows Eq. (33)

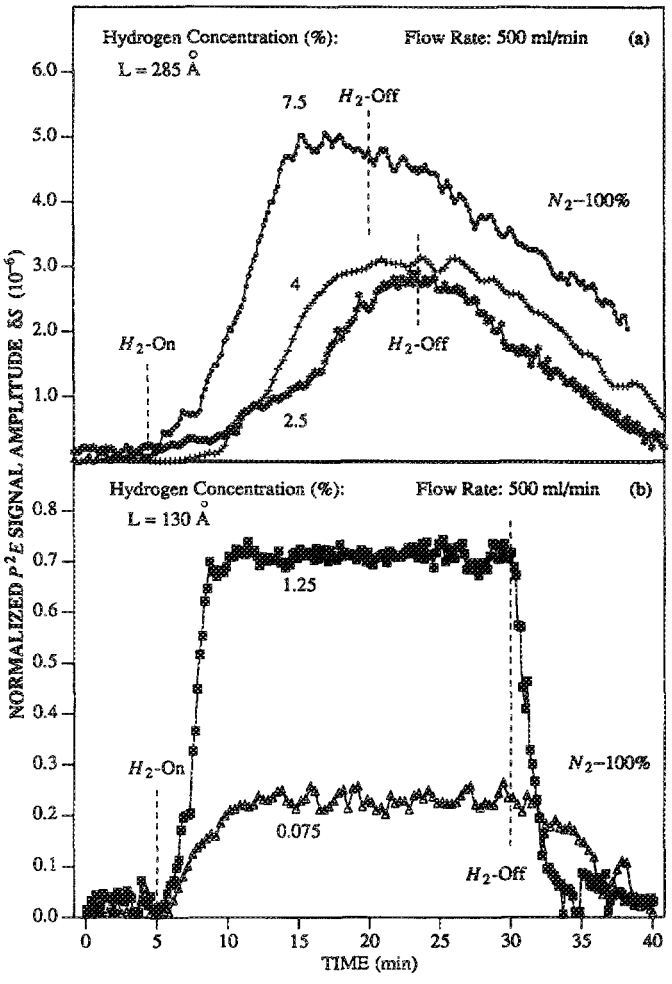

FIG. 7. Photopyroelectric responses as a function of time, for two concentrations of hydrogen in nitrogen ($T = 20$ °C; flow rate; 500 ml/min;). (a) 2.5%–7.5% hydrogen in nitrogen (Pd thickness = 285 Å); (b) 1.25% and 0.075% hydrogen to nitrogen (Pd thickness = 130 Å) (from Refs. 25–27).

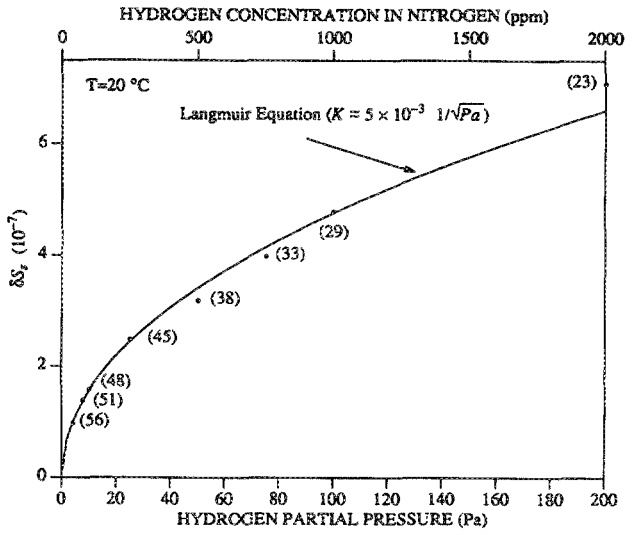

FIG. 8. Variation of output differential saturated signal amplitude δS_s as a function of hydrogen concentration and Langmuirian isotherm fit to the data, as per Eq. (33) ($T = 20$ °C; Palladium thickness: 130 Å). Parentheses: Response time at shown hydrogen partial pressure in minutes (from Ref. 29).

plotted vs P_{H_2} using $K(T) = 5\times10^{-3}$ Pa$^{-1/2}$. We note the good agreement between the Langmuir isotherm and the experimental points especially at low pressures, where the Langmuir behavior is expected to be strictly valid. No attempt was made by those authors to interpret any experimental results for concentrations higher than 2000 ppm (200 Pa)[27] because the use of the Langmuir isotherm for concentrations over 2 Torr (266 Pa) is quite problematic.[33]

4. Ultimate pressure sensitivity

From the general equation of the Langmuir isotherm[8–10] and the instrumental differential signal resolution ($\approx 10^{-8}$), the PPE sensor should be sensitive to a minimum coverage, Θ_{min}, at STP of approximately:[27]

$$\Theta_{min} = \frac{\delta S_{min}}{\delta S_{max}} \approx \frac{10^{-8}}{9\times10^{-6}} \approx 1.1\times10^{-3}. \qquad (34.1)$$

Using Eqs. (9) and (10) (with $\xi \equiv S$) and the minimum detectable coverage, it can be shown that the photopyroelectric sensor should have the lowest pressure sensitivity P_{lim}:[27]

$$P_{lim} = \left(\frac{\Theta_{min}}{K(T)(1-\Theta_{min})}\right)^2 \approx 0.2 \text{ Pa} \qquad (34.2)$$

which corresponds to 2 ppm. This estimate was found to be 20 times below the experimental sensitivity limit of 40 ppm of hydrogen in nitrogen.[27,28] This discrepancy was attributed to the fact that the instrumental detection limit of 2 ppm is valid for measurements without any interferences from other gases, and not under flow-through conditions. The potential sensitivity of the photopyroelectric sensor, however, to such low hydrogen partial pressures makes it a promising detection device for trace hydrogen gas analysis under STP

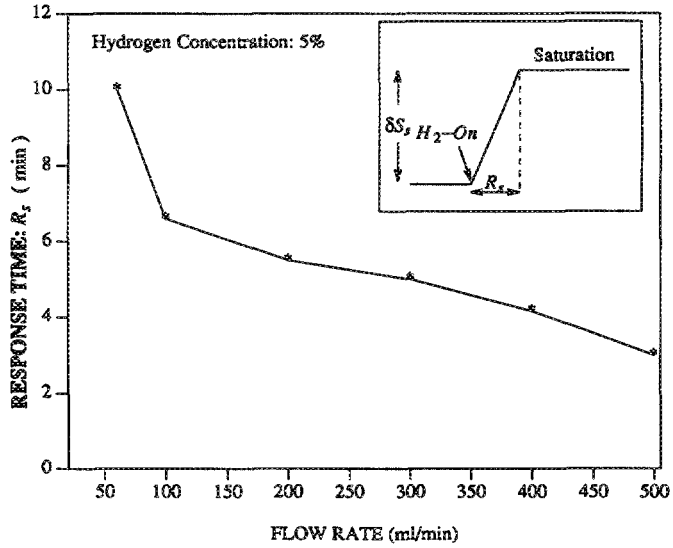

FIG. 9. Variation of output differential signal amplitude δS_s response delay for various hydrogen flow rates (60–500 ml/min; $T = 20$ °C) (from Refs. 25 and 26).

conditions. Most importantly, the lowest (40 ppm) hydrogen concentration signal is not believed to be an absolute instrumental minimum under STP.[27] It ought to be mentioned that the reported sensitivity of the dc pyroelectric sensor is 1% (10^4 ppm).[22,24]

5. Detector characteristics

To date the behavior of several Pd thicknesses (35–1600 Å) has been studied under various hydrogen concentrations.[22] It is worthwhile to note that thicknesses close to 130 Å seem to be the most suitable for the photopyroelectric detector. Palladium films thicker than 1000 Å and thinner than 100 Å have been found not to be sensitive to hydrogen concentrations less than 1%. Amico *et al.*[35] described a similar phenomenon for their surface acoustic wave sensor but with a different thickness range (1900–7600 Å) (see Sec. III B below).

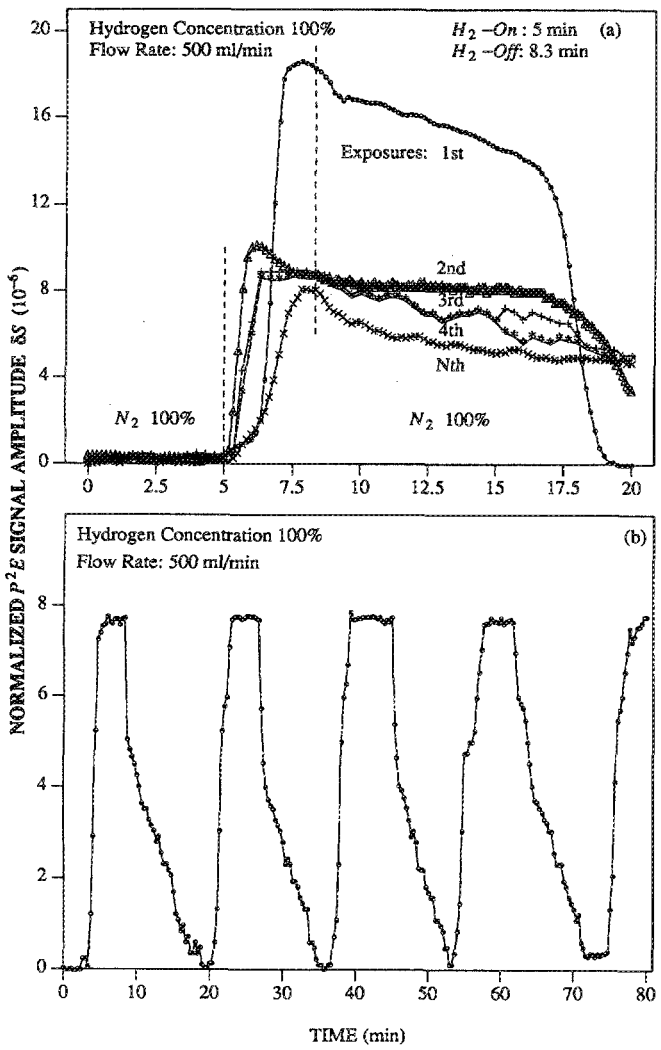

FIG. 10. Variation of the output photopyroelectric signal δS as a function of time, after several exposures to pure hydrogen: (a) With an as-received Pd-PVDF 285-Å film; (b) With a previously exposed Pd-PVDF 285-Å film (from Refs. 26–28).

Using 285-Å Pd thickness as an empirical guess, the experimental results showed that the photopyroelectric sensor hydrogen detection ability is completely reversible and durable. Initially, one face of the Pd-PVDF film was exposed several times to 100% H_2 (100 kPa). The experimental curves in Fig. 10(a) show an irreversible sensitivity loss with each successive introduction of hydrogen up to the 4th exposure, with well-reproducible responses upon further exposures. A similar phenomenon has been observed by Lalauze *et al.*[36] who used pure Pd substrates in order to study the influence of the surface state of a thin film of Pd on the H_2 diffusion process. The phenomenon concerning the pressure-concentration (*P-C*) isotherms as a function of the cycle of exposure to H_2 has also been reported by Qian and Northwood.[37] These authors have shown that, after 5–10 absorption-desorption cycles, the irreversibility does not persist on further absorption-desorption cycles, and this seems to be in direct relation with observations reported on the Pd photopyroelectric sensor.[26,27] According to Lalauze *et al.*[36] however, sample treatment (exposure to H_2 and heat treatment) has a large influence on hydrogen adsorption. The Pd-PVDF photopyroelectric signal saturated at a reproducible value after four or five exposures [Fig. 10(a)] without any additional treatment, unlike the work by Lalauze *et al.*,[36] who reported stabilization only after a relatively sophisticated treatment program had been followed. The stability of the Pd-PVDF photopyroelectric sensor has been repeatedly confirmed with various Pd-PVDF films.[26,27] Figure 10(b) shows the excellent reproducibility of the signal after many exposures to pure hydrogen following the first five "break-in" exposures. This signal level has been found to be very reversible and reproducible with several Pd-PVDF films. In terms of durability, the basic signal quality shown in Fig. 10(b) lasted even after several hundred exposures, as well as under various hydrogen concentrations. Thus, reproducibility and durability of the photopyroelectric sensor has been successfully demonstrated,[26] along with very good economic yield, considering that a 10 cm × 15 cm palladianized sheet of PVDF (approximately $100)[32] may supply 100–150 active elements, each of which can be simply inserted in the Inficon housing to replace an old element and generate a new detector.[32]

The direct signal dependence on heat of adsorption due to heat released to the Pd surface, following adsorption, is the dominant mechanism of the dc pyroelectric sensor, which, however, does not register in the synchronous detection mode of the ac device. Heat of adsorption will not register in the lock-in amplifier, nor will opening and closing the valve during gas flow cycles, thus rendering the ac device immune to several potential pitfalls of the dc pyroelectric sensor.[22,24]

III. PIEZOELECTRIC SENSORS

A. Piezoelectric quartz crystal microbalance (PQCMB) sensor

1. Introduction and historical perspective

One gas detection device, which has proved to be very useful, is the piezoelectric quartz crystal microbalance

(PQCMB). King[38–41] showed experimentally that a coated quartz piezoelectric crystal could be used as a sorption detector. The detector principle is well known and was described by Sauerbrey as early as 1959.[42,43] The oscillation frequency of a quartz crystal depends on the total mass of the crystal, and that of any coating layers (or electrodes) on the crystal surfaces. When adsorbed gas molecules are absorbed in the thin coating layer, the resonance frequency decreases in proportion to the mole number of dissolved molecules. Thus, the concentration of a pollutant gas is measured by detecting a change in the crystal vibration frequency.

In recent years, coated piezoelectric crystals have demonstrated good efficiency as detectors of various pollutants. Several workers[44–48] have used coated crystals as sensors for sulfur dioxide (SO_2) pollution. The piezoelectric sensor has also been used by Karmarkar and Guilbault for the detection of ammonia (NH_3) and nitrogen dioxide (NO_2);[49] by Hlavay and Guilbault[50] for the detection of hydrogen chloride (HCl); and by others [51] for hydrocarbon compound detection. The ability of coated piezoelectric crystals to detect organophosphorous compounds has also been demonstrated.[52,53] Piezoelectric crystal detectors for explosives and mercury (Hg) have been described by several authors.[54–56] Recently, Deakin and Byrd have used a coated quartz crystal for the detection of electroinactive cations in aqueous solution.[57] Relative humidity measurements using a PQCMB have been performed by Randin and Zulling.[58] Lee *et al.*[59] have used coated crystals for the detection of water in gases. The effect of air and gas pressure on the vibration of miniature quartz tuning forks has been investigated by Christen in 1983.[60]

In this section, we review some of the most important points concerning the detection of hydrogen in a flow-through system by a Pd-coated piezoelectric quartz crystal microbalance.[61–63] The influence of system parameters that affect the physico-chemical mechanism of the sensor response is described. A discussion of the drawbacks of the piezoelectric detector is also reported.

2. Theoretical background

The resonant frequency of a quartz crystal is dependent on the geometric dimensions of the quartz plate and the thickness of its electrodes. The principle of the quartz crystal sorption detectors is simple: When gas molecules are absorbed in a thin coating layer, which is chosen according to the desired gas selectivity on a quartz crystal surface, the decrease in resonance frequency is in proportion to the quantity of dissolved molecules. The theory which is outlined below, was originally developed by Sauerbrey.[42,43] The application of an electrical field on the quartz crystal gives rise to a resonance frequency, F, which can be expressed as[42,43,64]

$$F = N_F/z, \tag{35}$$

where N_F is a frequency constant equal to half of the transverse wave propagation velocity in the plane of the crystal and z is the thickness of the crystal. The relation between the frequency change ΔF and the crystal thickness variation Δt is given by[42,43]

$$\Delta F/F = -\Delta z/z. \tag{36.1}$$

Equation (36.1) can also be written as

$$\Delta F/F = -\Delta M/A_0 \rho z, \tag{36.2}$$

where ΔM is the change of the mass of the quartz crystal due to the absorption of the gas, A_0 is its surface area and ρ is the density of the quartz ($= 2.6\ \mathrm{g\ cm^{-3}}$).[64] Using the frequency constant $N_F = 0.1679\ \mathrm{MHz\ cm^{-1}}$ for AT-cut quartz,[42] one finds

$$\Delta F(\mathrm{Hz}) = -2.3\times 10^6\ F^2(\Delta M/A_0), \tag{37.1}$$

where now F is the resonant frequency (MHz) of the crystal in the absence of gas absorption, ΔM is the mass of the absorbed gas molecules (g) and A_0 is the total surface area ($\mathrm{cm^2}$). The minus sign conveniently indicates a decrease of F with increasing mass of the quartz crystal. Equation (36) can also be expressed as a function of concentration:[51,65]

$$\Delta F = -K_c \Delta C_0, \tag{37.2}$$

where K_c is a constant related to the resonant frequency of the coated quartz plate, and it includes a conversion factor between the mass of the absorbed gas (g) and the concentration ΔC_0 (ppm or %), of the gas in the gas phase. Thus, Eq. (36.2) becomes[65]

$$\Delta F/F = -\Delta M/M, \tag{38}$$

where the total mass before any absorption of gas is[64] $M = M_{PG} + M_{\mathrm{Pd}}$; M_{PG} is the mass of the piezoelectric crystal and M_{Pd} is the mass of the chemically sensitive layer (Pd in this case). In general, in the experiments which have been reported to date, the minimum measurable frequency shift was on the order of 0.1–1 Hz. The masses of the Pd-coated quartz crystal were approximately 80–100 mg and their resonant frequencies, F, were 5–12 MHz. Under these conditions, Eq. (38) shows that the minimum detectable mass of absorbed gas by the Pd layer is $\Delta M \approx 1 - 2\times 10^{-8}$ g. The theoretical detection limit for the piezoelectric quartz crystal detector appears not to have been calculated rigorously from first principles. Sauerbrey estimated this limit to be approximately 10^{-12} g.[43] King's estimation was approximately 10^{-9} g.[38] It is obvious from Eq. (38) that mass sensitivity is better for detectors with high resonance frequency, F.

3. Experiment and results

A literature survey clearly shows that the science and technology of the detection of H_2 by the piezoelectric quartz crystal coated with Pd electrodes has not progressed quite as rapidly as other above-mentioned detection schemes. It is likely that the complex mechanisms of the hydrogen-palladium system[6,66–70] and the strong interference of oxygen-Pd reactions[71–74] have made quantitative aspects of this investigation very problematic. Frazier and Glosser[75] have used a quartz crystal in order to determine the quantity of hydrogen absorbed by an evaporated palladium film. Bucur *et al.* have used a PQCMB at 80.3 °C to study the kinetics of hydrogen sorption by thin Pd layers.[76] The mechanism of hydrogen sorption by thin palladium layers has also been studied at a temperature of 61.1 °C.[77] Under ultrahigh vacuum (UHV) conditions, Bucur has further used a PQCMB in

order to study the effect of CS_2 molecules on the desorption kinetics of hydrogen from a thin Pd layer at 59.6 °C.[78] Measurements for H_2-O_2 reactions using the piezoelectric quartz crystal under UHV conditions have also been performed.[79] Mecea and Bucur have used the piezoelectric device for sorption studies under dynamic conditions.[80] The experimental setup of a typical flow-through H_2 detection instrument using the piezoelectric quartz crystal detector is shown schematically in Fig. 11. The piezoelectric instrumentation consisted of an oscillator powered by a regulated power supply. The applied voltage is usually kept constant (10–20 V dc). The frequency output from the oscillator was measured by a frequency counter. The response of the Pd-PQCMB sensor could be observed as a change in the resonance frequency of the crystal,[42,43] in agreement with the simple theoretical considerations presented above. Abe and Hosoya[61] have used a piezoelectric quartz crystal for the detection of flowing hydrogen both in ambient air and in nitrogen (0.5% H_2 in N_2 and in air). Their limited study, however, did not lead to definite quantitative conclusions about the hydrogen detection capabilities and operating mechanisms of the Pd-PQCMB sensor.

a. Influence of the Pd thickness. It is important to point out that the thickness of the Pd coating/electrode plays an important role in the operation of the detector. Frazier and Glosser have shown the influence of the Pd thickness on the piezoelectric measurements in the range of 60–1200 Å at 27 °C.[81] They also showed that the phase transition of the Pd depends strongly on its thickness.[81] Figure 12 shows the reduced pressure-concentration (P-C) absorption isotherms for Pd-hydrides obtained by the above authors.

b. Sensitivity and limitations. We are going to describe some recent experiments showing how problematic is the detection of hydrogen by a quartz microbalance at room temperature under flow-through conditions.[60-63] It has been realized[61] that the pretreatment of the detector prior to any experiments plays an important role in their interpretation. Initially, a Pd-PQCMB sensor was left for several days under ambient conditions in order to observe the influence of atmospheric air on the catalyst.[61] Afterwards, hydrogen ($[H_2] = 30\%$ in N_2) was introduced into the test cell. Figure 13 shows the variation of the resonance frequency (an

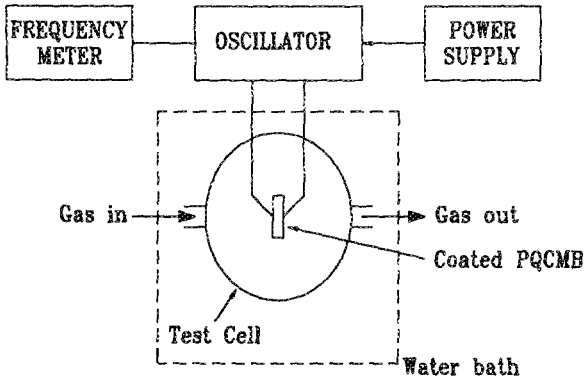

FIG. 11. Electronic setup of the PQCMB detector.

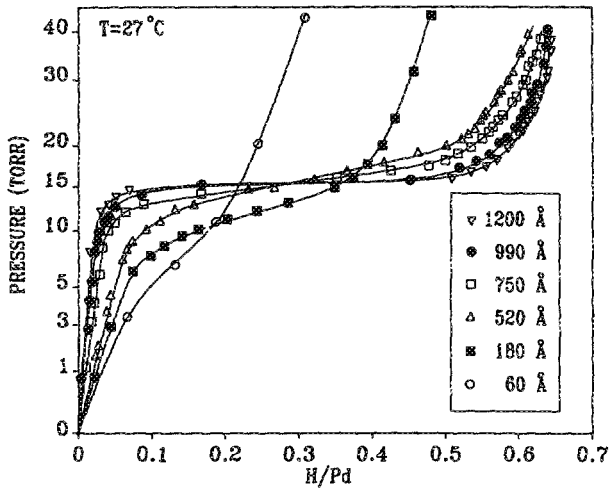

FIG. 12. Pressure-concentration isotherms for Pd hydride for various thicknesses (from Ref. 81).

increase in ΔF) as a function of time. A signal decay toward the baseline was observed upon closing the inlet valve and evacuating the test call, as expected. The phenomenon of a positive ΔF shift upon H_2 exposure is surprising in the light of the simple accepted theory presented in section above; however, it has been observed by both Christofides and Mandelis[62] and Abe and Hosoya,[61] who used as flowing gas mixtures of hydrogen 0.5% in air and nitrogen. Figure 14 shows some of the experimental results[61] concerning the adsorption-desorption curves, which indicate the increase of ΔF after adsorption-absorption of hydrogen. It has been hypothesized[61] that the ambient oxygen plays an important role in the Pd-PQCMB response: Preadsorbed O_2 on the Pd

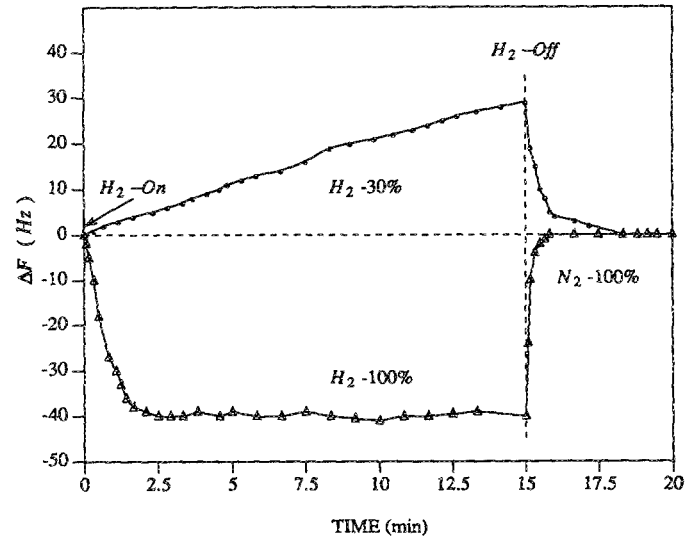

FIG. 13. Piezoelectric quartz crystal responses as a function of time, for two different concentrations of hydrogen in nitrogen: 30% and 100%. The test-cell was exposed for several days to the laboratory ambient air before the first experiment ($F = 6$ MHz; Pd thickness: 800 Å; flow rate: 500 ml/min; $T = 20$ °C) (from Ref. 62).

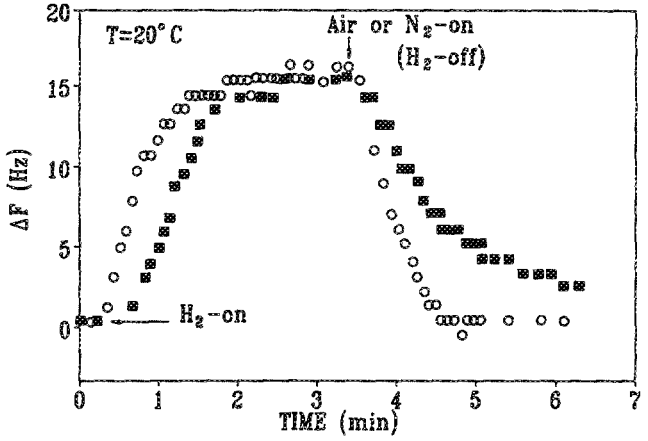

FIG. 14. Piezoelectric quartz crystal responses as a function of time (F = 6 MHz; Pd thickness: 1500 Å; flow rate: 266 ml/min): (■) 5120-ppm hydrogen in nitrogen; (○) 5120-ppm hydrogen in air (from Ref. 61).

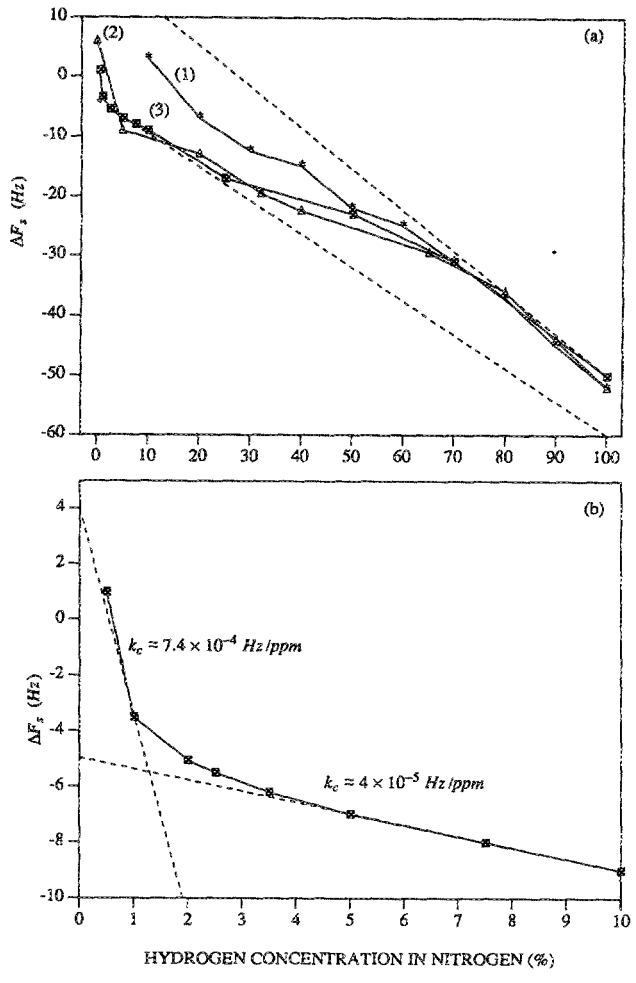

FIG. 15. (a) Variation of the saturation resonance frequency shift, ΔF_s, with hydrogen concentration (or partial pressure). The three curves were obtained from the original exposure where the presence of ambient air before the onset of the experiment was significant: ΔF_s of curve (1) (unpurged) is consequently smaller than that of curves (2) and (3) where the cell was purged with N_2 before the experiment (from Ref. 61). (b) Variation of the saturation resonance frequency shift, ΔF_s, as a function of hydrogen partial pressure and concentration of hydrogen in nitrogen in the range of 0.1%–10% hydrogen in N_2 (from Ref. 62).

surface reacts with the introduced H_2 gas and forms H_2O which leaves the Pd surface via evaporation. Therefore, the weight of the quartz crystal decreases as a result of the H_2-O_2 reaction, which is consistent with a positive ΔF. Vannice *et al.*[73] have studied the absorption of H_2 and O_2 on platinum black. The great similarity between Pt and Pd concerning the absorption of H_2 and O_2 in these metals allows a reasonable comparison to be made between the results by Vannice *et al.*,[73] the hypothesis put forth by Abe and Hosoya,[61] as well as the observations by Christofides and Mandelis:[62] The water formed during the reaction leaves the surface, and, in doing so, it is not replaced by additional hydrogen.[61] The following empirical chemical reactions describe the possible mechanism on the Pd surface:[33] Dissociation-recombination of oxygen,

$$O_2 \rightarrow 2O_a, \tag{39a}$$

followed by dissociation-recombination of hydrogen,

$$H_2 \rightarrow 2H_a \tag{39b}$$

and finally resulting in water formation,

$$O_2 + 2H_a \rightarrow 2OH_a \tag{39c}$$

$$OH_a + H_a \rightarrow H_2O_{(g)}. \tag{39d}$$

According to Ponec *et al.*[71] the reaction between hydrogen and oxygen at the Pd surface at 0 °C goes to completion producing desorbable water, in agreement with the last step, reaction (39d), of the four-step mechanism (39). However, according to Lundström *et al.*,[33] the details of the water-production reactions on the palladium layer are still not known. This phenomenon turned out to be a significant disadvantage of the piezoelectric quartz crystal detector. The results obtained with the 30% H_2 in N_2, Fig. 13, indicate that gas impurities in the flowing gas mixture, notably oxygen, may play the dominant role in the response of the sensor.

The relationship between gas concentration and Pd-PQCMB detector response, ΔF, is an important parameter for sensor characterization. Figure 15(a) shows the variation of saturation resonance frequency, ΔF_s, as a function of gas phase hydrogen concentration.[61] Unlike the prediction of Eq. (37), there are three apparent response regimes; a nonlinear one at concentrations between 20 and 70%, and two linear regimes at low ($<20\%$) and high ($>70\%$) concentrations, a region where all experimental curves converge. This convergence of all the experimental data can be explained by assuming that at high pressures the adsorbed and absorbed hydrogen dominates all other interfering phenomena. The presence of trace oxygen is thought to be partly responsible for the deviation of the Pd-PQCMB sensor response at low concentrations. Figure 15(a) indicates that the purging history of the test cell plays an important role in determining the $\Delta F_s([H_2])$ curve at lower ($\leqslant 70\%$) concentrations. An important factor is the initial irreversible sensitization of the Pd-PQCMB surface with increasing degree of exposure to hydrogen flow. Figure 15(b) shows the variation of the saturation, ΔF_s, as a function of gas phase

hydrogen concentration[62] in the range of 0.1–10% H_2 in N_2. Unlike the response predicted by Eq. (37), there are two apparent linear response regions; one with the slope $k_c \approx 7.4\times10^{-4}$ Hz/ppm at low concentrations ($<2\%$) and another one at higher concentrations (3–10%) with the slope $k_c \approx 4\times10^{-4}$ Hz/ppm. The presence of trace oxygen even after the evacuation of atmospheric air with the help of N_2 seems to be partly responsible for the deviation of the Pd-PQCMB sensor response and the positive ΔF_s at low concentrations.[61,62] In fact at very low hydrogen concentrations many impurities such as oxygen may still exist on the Pd surface even after several activation cycles. On the other hand, for higher H_2 concentrations, clean surface area will be generated due to the reduction of the oxygen layer. The low-concentration anomalous behavior {between 20% and 70% [see Fig. 15(a), curves (2) and (3)]} could be due to the $\alpha \rightarrow \beta$ phase transition which takes place around 20 kPa. According to Lundström *et al.*[33] it is probable that a phase transition from α to β may also take place at low temperatures and high concentrations (1%–100%).[82] This is in disagreement with other evidence[6] showing the possibility that at room temperature the phase transition takes place around 2% (2 kPa). It is also well known that the phase transition depends on the palladium thickness,[81] a complicating factor. Another problem for a quantitative analysis may be the presence of water on the Pd layer at room temperature. This could cause the Pd layer to be saturated at low pressures, as was observed in studies under UHV conditions.[33]

c. The influence of temperature and flow rate. The temperature variation during the gas detection by the Pd-PQCMB plays an important role because of the influence of temperature on the quartz crystal operation. According to Sauerbrey,[42] if a piezoelectric AT-cut or BT-cut crystal undergoes a temperature change, a significant variation of resonance frequency, F, could be expected. Abe and Hosoya[61] reported a variation of 0.75 Hz/°C in the range of 15–30 °C: Figure 16(a) presents the effect of temperature on the resonant frequency of Pd-PQCMB device. Christofides and Mandelis[62,63] have also reported a nonmonotonic dependence of resonant frequency shift on temperature of the Pd-PQCMB in the presence of pure hydrogen, Fig. 16(b). In Fig. 17 one can note that at relatively high temperatures the Pd-PQCMB is more sensitive than at room temperature (350 ppm/Hz).

The effect of flow rate, W_r, on sensitivity and response time was measured[62,63] using 5% of hydrogen in nitrogen. The flow rate was varied from 60 to 700 ml/min. It was observed that W_r does not influence ΔF_s very much, and saturation occurs essentially at the same level (≈ 8 Hz). On the other hand, the response time, R_s, of the sensor increases monotonically (7–14 min) with decreasing flow rate between 600 and 60 ml/min as shown in Fig. 18. We note the R_s is strongly dependent on W_r, especially at low flow rates. At higher flow rates (>400 ml/min), the response time becomes essentially independent of flow-rate value. This observation has been made earlier by Cooper *et al.*[83] According to these authors the response time, R_s, is proportional to V_c/W_r[83] where V_c is the volume of the test cell (750 ml in our case). The experimental results on Fig. 18 do not follow a $1/W_r$ law. Cooper and co-workers[83,84] attributed a similar

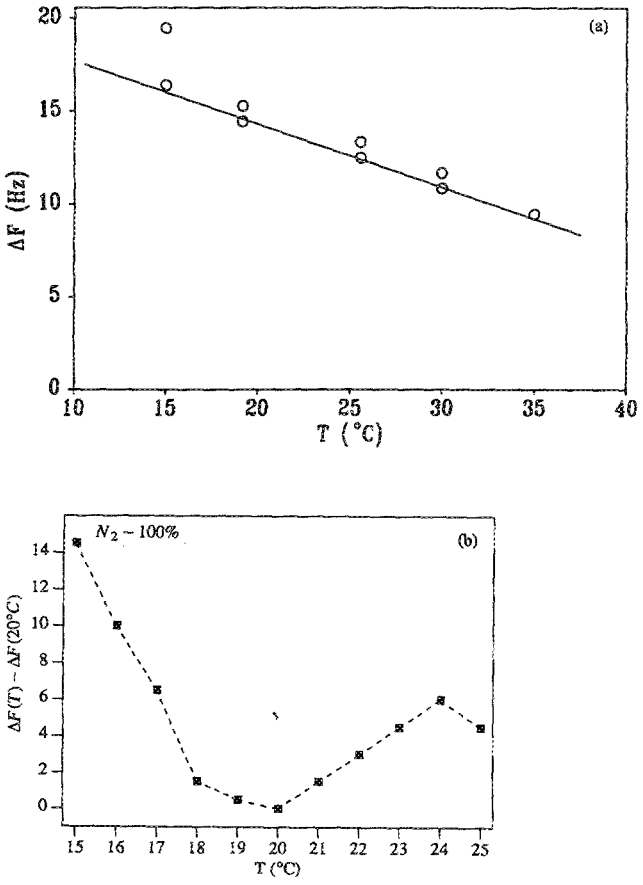

FIG. 16. (a) Effect of temperature on the sensitivity of the Pd-PQCMB device under exposure of 5120 ppm H_2 in N_2 (from Ref. 61). Overlapping data points correspond to experimental reproducibility. (b) Effect of temperature on frequency shift [$\Delta F(T) - \Delta F(20\,°C)$] vs T of the Pd-PQCMB device in pure N_2 (from Ref. 62).

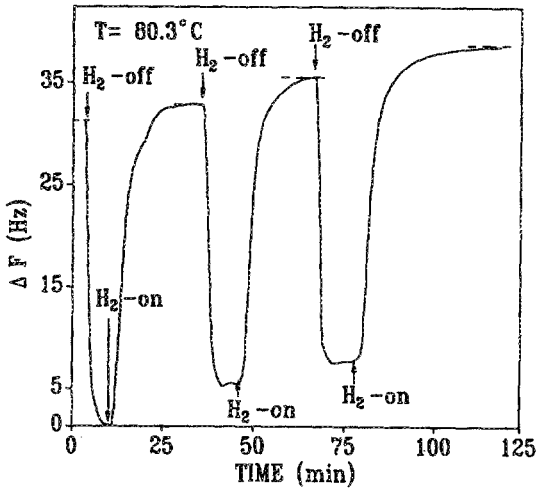

FIG. 17. Piezoelectric response as a function of time ($T = 80.3$ °C) (from Ref. 76).

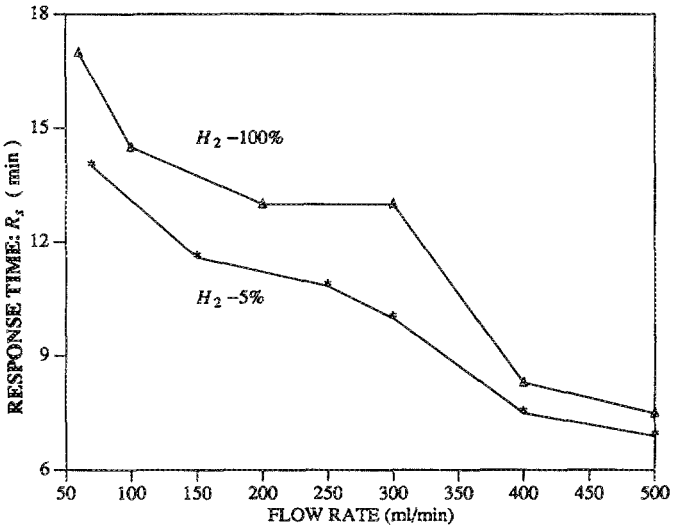

FIG. 18. Pd-PQCMB device resonance frequency shift variation as a function of time at 100% H_2 and 5% H_2 in N_2 for various flow rates: 70–500 ml/min. The hydrogen was turned on at $t = 0$ min ($T = 20$ °C) (from Ref. 62).

disagreement to a bad mixing of the detectable and carrier gas. The above results suggest that minimizing the test cell volume offers optimal responses of the Pd-PQCMB sensor.

B. Surface acoustic wave (SAW) detectors

1. Introduction and historical perspective

The mathematical basis of the phenomenon of surface acoustic waves (SAW) was published first by Lord Rayleigh in 1885.[85] At that time, SAW drew the attention of the scientific world and especially that of geologists because the acoustic energy released by earthquakes moves as a surface acoustic wave on the earth's crust. This natural type of waves is well known today as Rayleigh waves. The main characteristic of surface acoustic waves is that the acoustic field and particle displacement occur mainly on the surface of the solid. Almost a century had to pass in order for SAW to find their first application in electronics. In 1965 White and Voltmer[86] developed the interdigital transducers (IDT) which allowed the generation of Rayleigh surface waves in piezoelectric solids and then the application of SAW to radio-frequency signals. The main reason of the choice of Rayleigh waves among other kinds of surface acoustic waves such as Love and Stonely waves is that they are generated quite readily in a variety of piezoelectric materials using an IDT.

The dependence of wave velocities on temperature led to a temperature sensor based on a SAW delay line oscillator with a good linearity.[87] On the other hand, it is well known that SAW velocities can be strongly affected by stressing the crystal through which the wave travels.[88] This property led to the first SAW pressure sensor developed by Cullen and Reeder in 1975.[89] Two more SAW pressure sensor devices have been reported in 1980 and 1981.[90,91] Toda and Mizutani[92] and Joshi[93] reported the first SAW electric field sensor in 1983. They exploited the fact that an electrical field normal to the piezoelectric surface along which a SAW is propagating, causes a shift in the wave velocity because of the change in the stiffness of the crystal. At the same time several SAW voltmeters have been developed.[94–97] Hanna reported the SAW signal dependence on an applied magnetic field in 1987.[98] The SAW properties led to many other kinds of sensors during the last few years. The force and acceleration detector,[90,99–104] the displacement[105] and flow sensors,[106] and rotation (gyro-effect) SAW detector,[107] and others.

In recent years, considerable research effort has been directed toward the development of SAW gas sensors. In 1979, Wohltjen and Dessy,[108] reported the first SAW device for chemical vapor detection. A SAW sensor has been used by Zellers *et al.* for the detection of styrene vapor,[109] and by other workers for vapor detection.[110–112] A comparison of a bulk wave (piezoelectric quartz crystal) and a surface wave device for the detection of SO_2 has been made by Bryant *et al.*[113] (see Sec. III B 5). The ability of SAW devices to detect NH_3 has also been demonstrated.[114] The SAW detector for humidity monitoring has been described by Joshi and Brace,[115] and Brace *et al.*[116] SO_2 and H_2S have been detected by Bryant *et al.*[117] using SAW devices. It is important to note that recently Amico and Verona have published an excellent paper[118] which reported the year of development, device structure and substrate, and the detecting membranes of several SAW detectors.

While Wohltjen and Dessy's work led to the development of SAW gas sensors,[108] it was Amico *et al.*[119] who first demonstrated that a surface acoustic wave device with an appropriate chemically sensitive coating (Pd) could be employed as a hydrogen detector. In this section, we review the development of the SAW device and mainly the work of Amico *et al.*[35,119–121] who developed the capability of the Pd-SAW device as a hydrogen detector.

2. Theoretical background

The principle of the SAW detectors is simple:[122,123] When gas molecules are absorbed in a thin chemically coated layer, which is chosen according to the desired gas selectivity, they perturb the properties of the surface acoustic waves. Surface acoustic waves travel on the surface of the piezoelectric substrate. In other words, the energy of SAW is localized within one or two acoustic wavelengths of the surface. This property gives the SAW the possibility to interact easily and strongly with the medium adjacent to the surface. Wave-medium interaction is the main, necessary (but not sufficient) property which can lead to a gas detector. The second question for device applications is to choose among different kinds of SAW, such as Love, Stonely, and Rayleigh. According to Wohltjen[122] the primary reason for focusing on Rayleigh waves is that they are generated quite easily in many piezoelectric substrates using an interdigital transducer electrode. Thus, the generation of the SAW by IDT is followed by the propagation of the wave through a chemically selective coated layer. This wave-matter interaction causes a perturbation of the Rayleigh surface wave's characteristics, such as amplitude, phase, velocity, etc. The measurements of changes in the SAW characteristics is an indicator of the presence of a gas on the coating surface layer of the device. In essence there are three different modes of

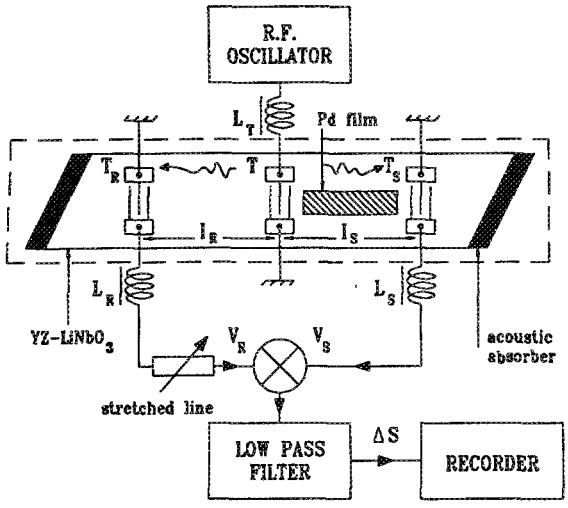

FIG. 19. Schematic diagram of the SAW detector set-up based on amplitude change (from Ref. 120). See text for description and details.

detection for monitoring gases: (i) Amplitude changes in the waveguiding layer take place because of the coupling of energy from the surface into the adjacent layer of gaseous matter; (ii) The velocity change of SAW propagation introduces phase shifts in the wave, and (iii) The resonant frequency, F, of the SAW device oscillator changes because of contact between the absorbed matter (gas) and the coating layer. In fact, there exists a relation between the fractional changes in the oscillation frequency, F, the acoustic velocity, U, and the phase delay Φ:[35]

$$\frac{\Delta F}{F}=\frac{\Delta\Phi}{\Phi}=-\frac{\Delta U}{U}. \tag{40}$$

a. SAW detector amplitude perturbations. A schematic representation of the SAW gas sensor based on amplitude change is shown in Fig. 19.[120] The operating characteristics of the detector are described in Table III. This SAW detector has been used by Amico *et al.*[119] for hydrogen detection. Surface acoustic waves were generated by an input transducer T and collected by two output transducers T_R, and T_S which were located at opposite sides of the YZ-$LiNbO_3$ substrate. The hydrogen Pd-SAW detector was fabricated on YZ-$LiNbO_3$ piezoelectric substrate. One of the propagation paths (l_s) was coated with a Pd thin film layer and acted as the selective layer of the device; on the other hand, the other path (l_R) was uncoated and it was used as a reference. The voltage outputs, V_s and V_R, through inductances L_s and L_R, were connected to a double-balanced mixer and then the output differential voltage, ΔS, was filtered out and recorded as[120]

$$\Delta S=V_R-V_S=V_M\sin(\Phi_R-\Phi_S)=V_M\sin(\Delta\Phi), \tag{41}$$

where V_M is the maximum output voltage (when $\Delta\Phi=K_n\pi/2$; K_n is an odd positive integer). From the wave propagation delay one may write the phase shift as[120]

$$\Delta\Phi=2\pi F\left(\frac{l_R}{U_R}-\frac{l_S}{U_s}\right)+\Phi_E, \tag{42}$$

where U_R and U_S are the velocities of the acoustic waves in the coated and noncoated surfaces, respectively, and Φ_E is the electric phase shift introduced by a stretched line used to adjust the initial phase difference $\Delta\Phi$ in order to minimize the differential output signal, ΔS ($\Delta S\rightarrow 0$). When adsorption-absorption (or desorption) of hydrogen takes place on the Pd surface, it changes the density and the elastic properties of the film which causes a shift on the SAW propagation velocity. As a consequence a voltage change is detected by the device as a function of hydrogen concentration C_0:[120]

$$\delta S=\frac{\partial V}{\partial C_0}=2\pi V_M\frac{Fl_s}{U_s^2}\left(\frac{\partial U_s}{\partial C_0}\right)\cos(\Delta\Phi). \tag{43}$$

As the argument of the cosine function was minimized ($\Delta\Phi\approx 0$) at the beginning of each experiment by the initial phase zeroing procedure, Eq. (43) can be expressed as

$$\delta S=2\pi V_M\frac{Fl_s}{U_s^2}\left(\frac{\partial U_s}{\partial C_0}\right). \tag{44}$$

We note in Eq. (44) that in the case of the SAW-amplitude detector for a given substrate material, the sensitivity depends on the $F\times l_s$ product, so it is clear that for a fixed sensitivity, the smaller the device to be fabricated, the higher its operating frequency, F.

b. SAW detector frequency (or velocity) perturbations. Wohltjen has shown that the shift frequency, ΔF, of a SAW gas detector can be expressed by the following relationship:[122,123]

$$\Delta F=(k_1+k_2)F^2L\rho-k_2F^2L(4\mu/U_R^2)\sigma, \tag{45}$$

where k_1 and k_2 are material constants for the SAW substrate (see Table IV),[124] L is the thickness of the Pd film, ρ is the film density ($m=\rho\times L$: mass per unit area) and $\sigma=(\lambda+\mu)/(\lambda+2\mu)$ (λ and μ are the film Lamè constants; in Eqs. (45) the dependence of the sensor response on the gas concentration is pronounced through the variation of m. In the case where the chemically selective layer is an elastomeric organic polymer, Eq. (45) may be simplified to[122]

$$\Delta F\approx(k_1+k_2)F^2(\Delta m/A_s), \tag{46}$$

where Δm is the absorbed gas mass and A_s is the surface of the coated layer. In Eq. (46) one can point out the analogy in form to Eq. (37.1) described in Sec. III A for the piezoelectric quartz crystal microbalance detectors. In Fig. 20 we show an experimental setup by Wohltjen *et al.*[123] for vapor detection using frequency-shift output. The same experi-

TABLE III. Operating characteristic of the Pd-SAW hydrogen detector. From Ref. 120.

Pd-SAW sensor characteristics	
Operating frequency, F (MHz)	75–76
Number of IDT finger pairs	5
Reference length, l_s (mm)	15.5
Pd Length, l_R	13.5
Pd thickness, L (mm)	3×10^{-4}

TABLE IV. Material constants for selected SAW substrates. From Ref. 124.

Substrate	V_R (m/s)	k_1 (m^2s/kg) $\times 10^{-8}$	k_2 (m^2s/kg) $\times 10^{-8}$
Y cut X propag. quartz	3159.3	− 9.33	− 4.16
Y cut Z propag. $LiNbO_3$	3487.7	− 3.77	− 1.73
Z cut X or Y propag. CdS	1702.2	− 8.33	− 2.67
Zcut X or Y ZnO	2639.4	− 5.47	− 2.06
Z cut X propag. Si	4921.2	− 9.53	− 6.33

mental setup has been used by Ballantine *et al.*[125] The SAW device was coated with a polymer layer and was exposed to small concentrations of dimethylmethylphosphonate (2 ppm) in dry air carrier stream at two operating frequencies (31 and 112 MHz). The dual configuration improved the detector stability against temperature and pressure changes.

3. Experimental results

In this section we will present data from Amico *et al.*[121] concerning the use of Pd-SAW sensor (see Fig. 19) for hydrogen detection as representative results to demonstrate the capabilities of these sensors. This study has been performed at atmospheric pressure and room-temperature conditions. The above authors have used the three conventional detection modes, amplitude, phase, and frequency for monitoring hydrogen gas. A system which allowed testing of the response of the SAW device in flowing H_2-N_2 mixture was used. Their system consisted of three subsystems: a gas control (three flow meters, input and output valves); a test cell, containing the Pd-coated surface acoustic wave detector (Pd-SAW); and an electronic shift amplitude analysis instrumentation [rf oscillator, low pass filter and recorder (see Fig. 19)].

The device was exposed to 0.1% H_2 in N_2 (flow rate = 810 ml/min) and the Pd-SAW response was monitored as a function of time. Typical experimental results are shown in Fig. 21. We note that it takes more than twenty minutes for the signal amplitude to reach saturation (δS_s). R_s denotes the saturation time. In Fig. 21 one can note that a few minutes after the introduction of hydrogen into the test cell the signal amplitude decreases as a function of time. The phenomenon of a negative amplitude shift upon H_2 exposure is surprising in the light of the discussion presented in the theoretical part of this section. No attempt by the authors to explain the decrease was made, however, it is possible that this phenomenon could be related to the anomalous behavior of the bulk piezoelectric quartz crystal (Pd-PQCMB) detector described in Sec. III A, through the effect of surface-absorbed gases other than H_2 interfering with SAW operation.

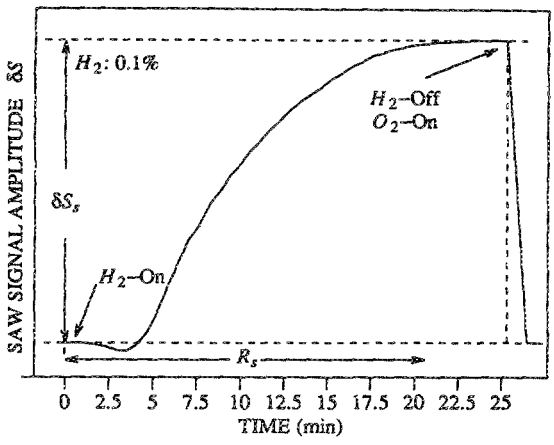

FIG. 21. Time response of the Pd-SAW hydrogen detector during the absorption and desorption process (H_2 flow rate: 828 ml/min; O_2 flow rate: 150 ml/min; $T = 20$ °C) (from Ref. 120). δS_s and R_s are defined in the text.

Figure 22 shows the variation of saturation response amplitude, δS_s, as a function of gas phase hydrogen concen-

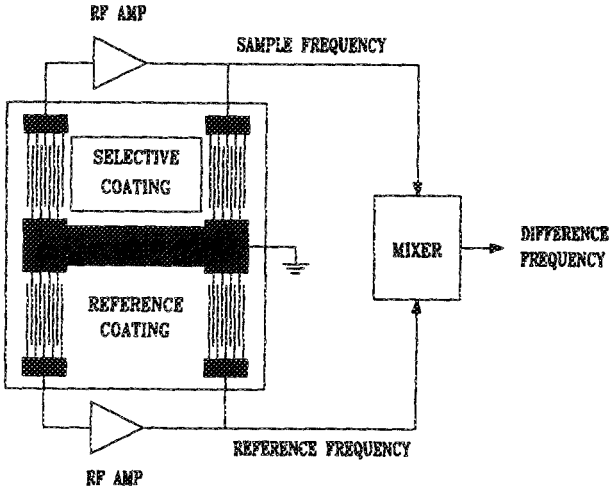

FIG. 20. Top view of SAW detector set-up based on frequency shift measurements (from Refs. 123 and 124).

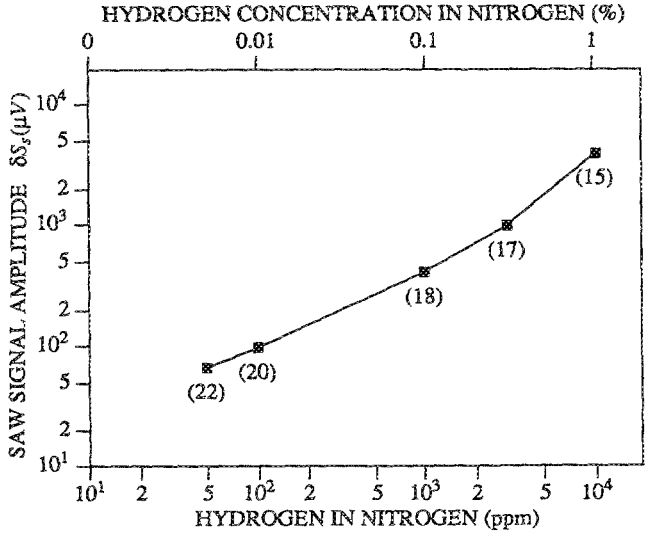

FIG. 22. Variation of the saturation SAW response δS_s, as a function of hydrogen concentration at 20 °C. Parentheses: Response time at shown hydrogen concentration in minutes (from Ref. 120).

tration in $N_2 + H_2$ fluxes in the range of 50–10^4 ppm, i.e., in the 0.005%–1% range of H_2 in N_2. The parentheses show the response time (in min) as a function of H_2 concentration. Contrary to the bulk wave piezoelectric detector [PQCMB (see Sec. III 1)] the Pd-SAW sensor response seems to be strongly influenced by the H_2 concentration at very low concentrations.

Amico *et al.*[35] have also studied the influence of the Pd thickness on the sensitivity of the Pd-SAW detector, as well as the influence of flow rate on its response time R_s. For this investigation the above authors have explored the velocity change, ΔU. In fact, using the relation between shift frequency and velocity change one can write

$$\Delta F/F = g\Delta U/U, \tag{47}$$

where $g = l_R/l_s$ is a geometrical factor. The net increase in mass due to the H_2-Pd reactions results in a decrease in the resonance frequency, F, of the coated oscillator. The experiments were performed using a frequency-shift detection technique which, according to several authors[35,121] is the most suitable for practical applications, because of its sensitivity and simplicity. The Pd-SAW hydrogen detector fabricated by Amico *et al.*[122] has the same characteristics as the one earlier[120] (see Table III) with the exception of different Pd thicknesses ($L = 1900$, 3800, and 7600 Å). Figure 23 shows the variation of $\Delta F/F$ as a function of Pd thickness, L, for two different H_2 concentrations. $\Delta F/F$ increases with increasing L. On the other hand, it can be seen that the relative frequency increase with H_2 concentration is not drastically influenced by the concentration, for a given Pd thickness.

Figure 24 shows the variation of the response time, R_s, as a function of the flow rate for three different H_2 concentrations. The flow rate does influence the response time of the sensor, which increases monotonically with decreasing flow rate between 810 and 8100 ml/min. Amico *et al.*[35] have also shown that there is an optimum Pd thickness for which

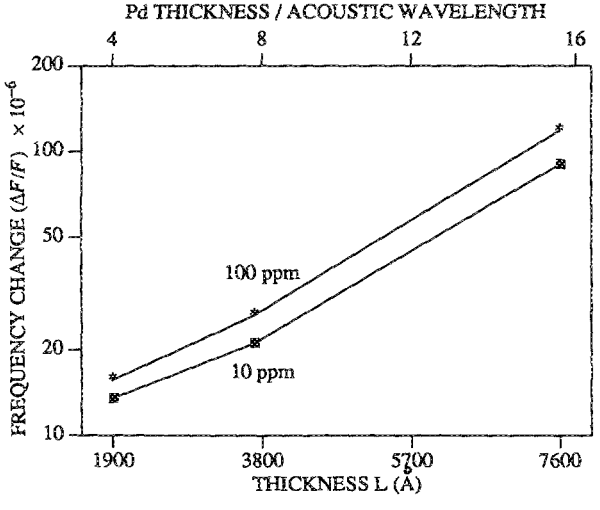

FIG. 23. Relative frequency change vs Pd thickness for two different concentrations of hydrogen in nitrogen for the Pd-SAW sensor fabricated by Amico, Palma, and Verona (from Ref. 35).

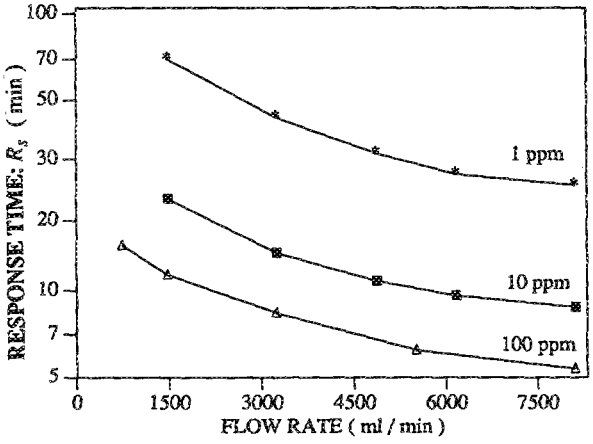

FIG. 24. Variation of the SAW response time, R_s, as a function of flow rate for three different hydrogen concentrations as measured for Pd film thickness $L = 7600$ Å, $T = 20$ °C (from Ref. 35).

R_s is minimum. According to these authors, among three thicknesses of Pd coating, 1900, 3800, and 7600 Å, it is the intermediate one (3800 Å) that presented the best Pd-SAW response, while the thinnest one presented the worst response.

4. Sensor characteristics

a. Sensitivity limit. As is shown in Eqs. (43)–(47) the sensitivity and the size of the SAW detectors are directly related to their operating resonance frequency. Thus, a device operating at 300 MHz presents a frequency shift 100 times greater than a 30-MHz device for the same absorbed gas mass [see Eq. (46)]. However, the baseline noise for the 300-MHz SAW device is higher than the one which operates at 30 MHz.[122] The reduction of the device area has implications with respect to the minimum mass change that can be detected by the SAW delay line oscillator. Some estimates of the SAW performances at various operating conditions are presented in Table V.

b. Temperature effect on SAW detector. An undesirable property of $LiNbO_3$ SAW oscillators is their high-temperature instability. According to Joshi and Brace,[115] the resonant frequency is found to decrease linearly with temperature with a slope of -6800 Hz/°C at $F = 75$ MHz while Ricco *et al.*[126] found this frequency shift to be -8800 Hz/°C at a resonance frequency of 110 MHz.

TABLE V. Estimated SAW device sensor performance. From Ref. 122.

Frequency (MHz)	Device area (cm^2)	Baseline noise (Hz)	Minimum detectable mass change (g)
30	1	3	3×10^{-9}
300	10^{-2}	30	3×10^{-12}
3000	10^{-4}	300	3×10^{-15}

5. Comparison between SAW and PQCMB detectors

It is well known that SAW and PQCMB detectors are mass sensitive and require a selective coating layer. These two detectors use a shift in acoustic wave resonant frequency (ΔF) as a signal. However, these two devices have two fundamental differences: (a) The resonant frequency of the SAW device can be a few hundred times higher than that of the PQCMB detector, which implies greater sensitivity. (b) The SAW device has the ability to occupy much less space than the PQCMB device. The reduction of device area has implications with regard to the minimum mass change that can be detected by a SAW delay line oscillator. According to Wohltjen,[122] for a *YX* quartz SAW delay line oscillator Eq. (46) can be written as

$$\Delta F = 1.3\times 10^6 F^2(\Delta M/A_s)\,. \tag{48}$$

It should be noted that the numerical factor of Eq. (48) is smaller than that of Eq. (36) for the PQCMB detector (see Sec. III A). However, since the operating frequency of the SAW device is much greater than that of the bulk wave detector, a compensation in sensitivity occurs (5000 ppm). A direct comparison between a 6-MHz bulk wave oscillator and a 75-MHz SAW oscillator shows that the SAW device theoretically should produce a much higher frequency shift. Actually, by term-to-term division of Eqs. (46) and (37.1) we have

$$\frac{\Delta F_{\mathrm{SAW}}}{\Delta F_{\mathrm{PQCMB}}} = \frac{1.3\times 10^6}{2.3\times 10^6}\,\frac{75^2}{6^2} \approx 88.3. \tag{49}$$

Equation (49) shows that the sensitivity of the SAW device is 88 times greater than that of the PQCMB device. This theoretical value was experimentally confirmed by the comparison between results by Amico *et al.*[120] for the Pd-SAW detector and those of the present authors[62] for the Pd-PQCMB device.

IV. FIBER OPTIC SENSORS (FOS)

A. Introduction and historical perspective

The concept of fiber optic sensors (FOS) is far from new. The first patents were obtained around the year 1965.[127] In the same year Gamble *et al.*[128] reported the use of fiber optics for a clinical cardiac characterization. However, using the background already obtained by the conventional gas analyzer spectrometers, serious research effort for the development of the fiber optic detector technology only started in the beginning of our decade.[129]

An optical fiber is essentially a "light pipe" or waveguide for optical frequencies. It is typically drawn from a spherical mirror to a diameter of a few to a hundred μm. A large variety of optical fibers is available from commercial manufacturers and these can be divided into five main types: All-polymer, silica, plastic-coated silica, glass fibers and fiber bundles.[127] One of the most valuable properties of an optical fiber is its flexibility, due to which it can be used for the transfer of an optical signal over distances of kilometers without the necessity of perfect alignment between source and detector and especially without any attenuations or signal degradation due to ambient electrical noise or electromagnetic interferences. This property, among others, led to many applications in the area of optical communication and in areas such as telephony and data transmission.

Recently there has been considerable research activity in the development of the fiber optic sensors in the field of sensing. The measurement basis in FOS consists of changing the features of light transmitted along the fiber, and these changes in turn are used to modify an output electrical signal in a receiver. FOS is a means whereby light guided within an optical fiber can be modified in response to an external physical, chemical, biological, or similar influence.

Detection of pressure with an optical fiber positioned in the arms of a Mach-Zehnder interferometer (see next subsection) has been reported by Hocker.[130] The measurement of pressure using optical fibers is effected by the variations in the relative phase between light propagating in the two interferometer arms. This variation of phase is attributed to the changes in the optical propagation characteristics in the arm exposed to the applied pressures.[130,131] On the other hand, the change in the optical fiber length due to thermal expansion or contraction, and the change induced by temperature in the refraction characteristics led to the development of the optical fiber temperature detector.[130] In 1981, Leslie *et al.*[132] reported the first fiber optic spectrophotometer in which the pressure sensing transducer was constructed using a fiber optical acoustic sensing coil in one of the arms of an interferometric fiber sensor. A fiber-optic hydrophone has also been reported.[131] While Yariv and Winsor[133] demonstrated theoretically the possibility of detecting weak magnetic fields by using an optical fiber with a magnetostrictive jacket, Jarzynski *et al.*[134] followed up with experimental verification. A fiber optic probe for pH monitoring was also reported by Peterson *et al.*[135] in 1980. In 1988, an optical fiber sensor, able to detect water and solvent in oil was reported by Smela and Ariles.[136] Fiber optic sensors for biomedical applications have been developed by Peterson and Vurek.[137]

In recent years, research efforts have been directed toward the development of gas fiber optic detectors. Optical fibers acting as light carriers, impact several attractive features in the chemical sensor field. In 1975, Hardy *et al.*,[138] reported the first FOS device for chemical gas detection. They used a FOS for the detection of cyanide (CN^{-5}) traces. One year later, David *et al.*[139] showed the ability of the FOS device to detect ammonia in ambient air. Giuliani *et al.*[140,141] have also detected ammonia vapor with an FOS device. The fiber optic sensor has further been used for the detection of oxygen, glucose, carbon, CH_4, carbon dioxide, and various other gases.[142] Several review papers concerning gas fiber optics describe in detail the development of many FOS for the detection of several gases.[143-146]

While the work of Hardy *et al.*[138] led to the fiber optic gas sensor, it was Butler[147] who first demonstrated that an FOS device with appropriate chemically sensitive coating (Pd) could be employed as a hydrogen detector. In this section, we review the development of the fiber optic hydrogen detector and mainly the work of Butler[147] and Butler and Ginley[148] which developed the capability of the Pd-FOS device as a hydrogen detector.

B. Theoretical background

We can distinguish two main kinds of FOS:[144–149] (i) *Extrinsic*: The light can be allowed to exit from the optical fiber and to interact with different media before continuing to further propagate inside the same or another optical fiber; and (ii) *Intrinsic*: The light continues to propagate in the optical fiber without any outside interaction (see Fig. 25).

The principle of the FOS for gas detection is straightforward: When gas molecules are absorbed in the coated fiber part, which is chosen according to the desired gas selectivity, they change the optical properties of the coated layer. Depending on the particular device, the optical property measured can be absorbance, reflectance, luminescence, or scattering. The propagation of the light in an optical fiber can be explained with various degrees of accuracy in terms of electromagnetic theory or geometric optics.

1. Light waveguiding

Figure 26 shows the principle of light propagation in an optical fiber with the refractive indices n_1 and n_2 for core and cladding, respectively. In the case of the optical fiber $n_1 > n_2$ in order to promote total internal reflection. An incident ray which reaches the fiber at an angle Ψ_i is reflected at the critical angle Ψ_c from the core/cladding interface, where Ψ_c is given by

$$\sin \Psi_c = n_2/n_1. \tag{50}$$

From geometric optics (Snell's law) it is easy to show that

$$n_0 \sin \Psi_i = \sqrt{n_1^2 - n_2^2}\,, \tag{51}$$

where n_0 is the refractive index of the medium external to the optical fiber ($n_0 = 1$ when the external medium is air). The right-hand side of Eq. (51) is known as the numerical aperture (NA) of the fiber. If the outside medium is air, then Eq. (51) can be rewritten as

$$\mathrm{NA} = \sin \Psi_i. \tag{52}$$

It is obvious from Fig. 26 that the light propagation in the optical fiber is dependent only upon the refractive indices of the core and cladding. A large difference in the values of these indices is necessary for a large acceptance angle;[127] for a typical fiber $\Psi_i \approx 1$.

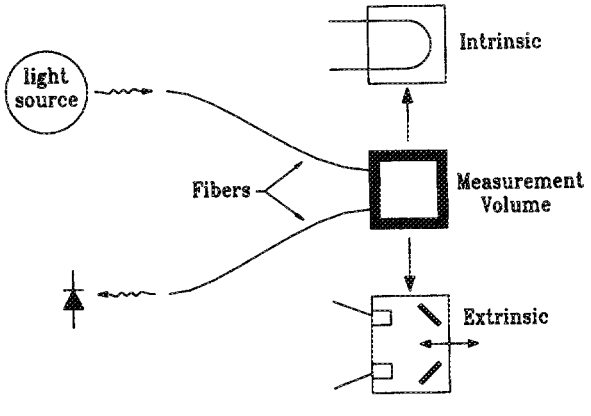

FIG. 25. Schematic diagram of intrinsic and extrinsic fiber optic sensors.

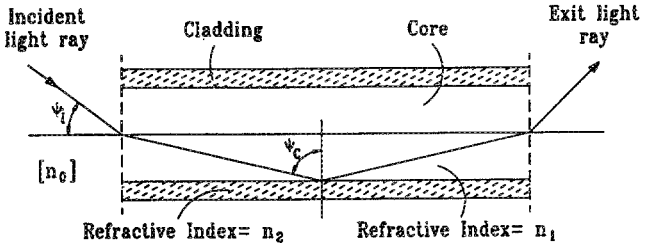

FIG. 26. Light propagation through an optical fiber (from Ref. 142).

2. Interferometric instrumentation

Interferometry is the most useful kind of measurement mode applied to the FOS technology. The physics of dual-beam interference is very old. However, the concept of this phenomenon is extremely useful in practice in the field of fiber optic detectors. It is well known that the maxima of the resulting fringe pattern appear where the phase difference between the interfering beams is $2K_n\pi$ (K_n is a positive integer). Any small perturbation in the phase of one of the beams due to external changes (temperature, pressure, magnetic field, chemical gas, etc.) will cause a transverse shift in position of the fringe pattern. According to Dakin and Culshaw[127] the resolution of modern optoelectronic techniques is about 10^{-4} of the fringe spacing, while according to Harmer[146] this resolution is even better and close to 10^{-6}. Many kinds of interferometer have been developed for gas detection; here we present the Mach–Zehnder interferometer (see Fig. 27) as a representative FOS technology.

In recent years special spectrometers have been developed for fiber optics in order to adapt them to FOS technology.[147,148] Conventional spectrometers have been modified to allow miniaturization, integration with the processing electronics, and multiple connection with many fibers at the same time. According to Laude *et al.*[150] a small modern spectrometer equipped with an optical fiber can be constructed from a small block of BK 7 glass; $20\times20\times98$ mm,[3] with a spherical mirror at one end and a grating at the other. An example of miniaturization of a FOS on a printed circuit card inside the electronics has been reported by Korth[151,152] and Tien and Capik.[153] In the experimental part of this section a new version of Mach–Zehnder interferometer will be shown using optical fibers instead of mirrors.[147,148] This version has been used for the development of FOS in the field with the advantage of detector portability.

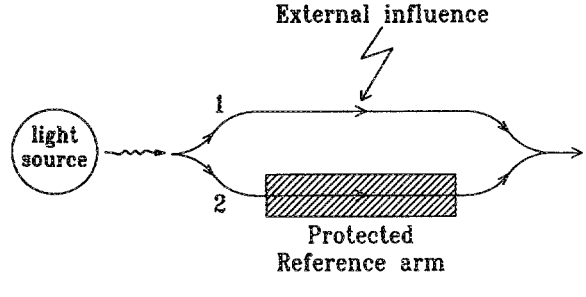

FIG. 27. Optical fiber Mach–Zehnder interferometer.

3. Measurement techniques

Fiber optic sensors for gas detection exhibit a large number of measurable parameters such as: refractivity, reflectivity, absorption, scattering, etc. In essence there are three main modes of detection for monitoring gases with FOS:[142]

a. Absorbance measurements. In this case the light intensity shift is determined by the quantity of absorbing species (gas molecules or atoms) in the optical path and is related to the Beer–Lambert relationship:[142]

$$A_I = \log(I_0/I) = m_a l C_0, \tag{53}$$

where A_I is the absorbance, I_0 and I are the incident and the transmitted light intensity, respectively, l is the path length of the light, C_0 is the concentration of the absorbing species, and m_a is the molar absorptivity. In the case that the medium and/or the selective chemistry used in FOS does not allow any transmission of the light, a measurement of the intensity of the reflected light may be used.

b. Reflectance measurements. The dependence of the optical characteristics of diffuse reflectance is a function of the composition of the system. According to the Kubelka-Munk theory[154] the reflectance R_0 of a semi-infinite medium is related to the absorption coefficient α and the scattering coefficient S_c (which is assumed to be independent of the concentration) through the relation

$$f(R_0) = \frac{(1-R_0)^2}{2R_0} = \frac{\alpha}{S_c} = m_a C_0, \tag{54}$$

where $f(R_0)$ is known as the Kubelka-Munk function in the semi-infinite sample.

c. Luminescence (or fluorescence) measurements. This kind of monitoring is very useful for detection of very low concentrations. The intensity of fluorescence I_F is given by the relationship[142]

$$I_F = E_x I_0 \Phi_F m_a l C_0, \tag{55}$$

where E_x is an experimental constant related to the instrumentation and sensor configuration, and Φ_F is the quantum yield of fluorescence. The linearity of Eq. (55) as a function of C_0 is violated at high concentrations.

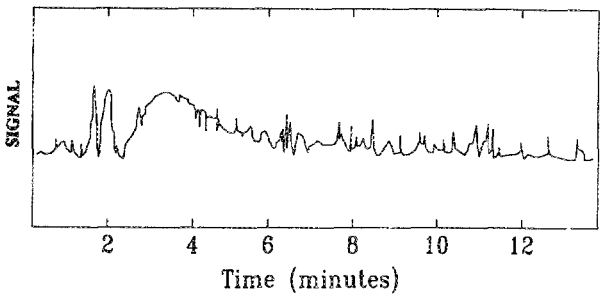

FIG. 29. Pd-FOS response as a function of time, for 0.6% of hydrogen in nitrogen (flow rate: 400 ml/min) (from Ref. 147).

C. Experimental results-hydrogen detection

In this subsection we will present experimental results concerning the use of a Pd-coated fiber optic detector (Pd-FOS) for hydrogen detection.[147] A Mach–Zehnder interferometer has been used. The experimental setup is shown in Fig. 28. Both ends of the coated and uncoated fibers are glued to a fused quartz plate with Eastman 910 adhesive. A more detailed description of the apparatus has been given by Butler and Ginley in 1988.[155] The Pd coating was made with the sputtering method and the thickness was 1.5 μm.[148] As is described by Butler, because of the close match in index of refraction, this makes an effective mode stripper. The light of a 0.5-mW He-Ne laser is split into two directions: One through the Pd-coated fiber and the other through the uncoated fiber. Both are exposed to the gas flow (fiber diameter: 80 μm). As shown in Fig. 29, the movement of the fringe pattern can be observed visually or by use of a simple photodetector and chart detector. Figure 29 presents the Pd-FOS response as a function of time for 0.6% of H_2 in N_2. The movement of the fringe pattern by one fringe corresponds to a change in optical path length of the arm of the interferometer by one wavelength of light. According to Butler the introduction of hydrogen (0.6%) in the test cell volume of approximately 75 ml gas causes the passage of three fringes (therefore one fringe corresponds to 0.2% H_2 in N_2). In

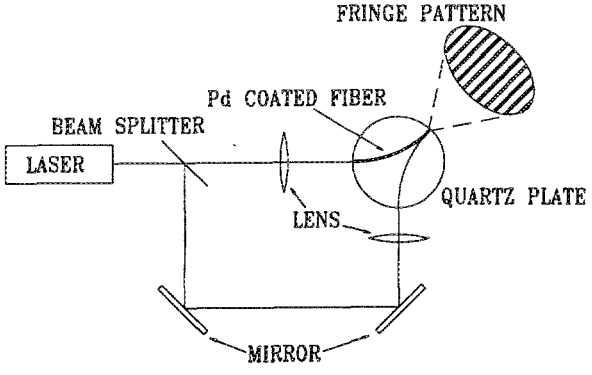

FIG. 28. Schematic of the Mach–Zehnder interferometer used for hydrogen gas detection by Butler (from Ref. 147).

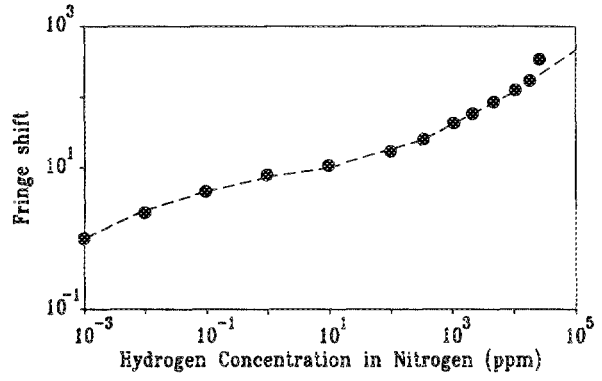

FIG. 30. The fringe shift for the Pd-FOS detector vs hydrogen concentration (from Ref. 148).

1988 Butler and Ginley[148] performed some new experiments using a hydrogen-sensitive palladium-coated optical fiber in the range of 20 ppb–10^4 ppm under STP conditions in nitrogen gas which presents a record of sensitivity to the H_2 gas under flow-through and STP conditions. Figure 30 presents the response of the Pd-FOS detector in a wide range of hydrogen concentration in N_2. In this figure one can note that the authors reported results up to 1 ppb, although the lower limit of sensitivity was estimated to be a few ppb. This estimation seems to be realistic due to the fact that early measurement capabilities achieved lower resolution than modern optoelectronic techniques:[148] the latter can measure better than 10^{-4} of the fringe spacing. This phenomenon is reversible and a similar behavior is observed when H_2 is removed from the Pd film. The temperature fluctuation effects were found to be equivalent to 2 ppm H_2/°C. This noise level could potentially limit the excellent resolution of the FOS. Thus the position of the fringes as a function of time gives much information on the kinetics of interaction of the Pd-H_2 system.

In order to interpret his experimental results, Butler[147,148] limited his analysis to the pressure regime where only the α phase (of Pd) exists. Then, by using a theoretical relationship between the hydrogen partial pressure, P_{H_2}, and the hydride composition in the Pd, he expressed the axial and radial strains as functions of Pd coating thickness in units of optical fiber radius. Butler used the Hughes and Jarzynski[131] relation

$$\Delta\phi/\phi = w - (n^2/2)\,[2u(P_{11} - P_{44}) + w(P_{11} - P_{44})]\,, \tag{56}$$

where $n = 1.46$ is the index of the refraction at the fiber center, P_{11} and P_{42} are the Pockels' coefficients and are equal to 0.1254 and 0.0718, respectively, and u and w depend on the Pd thickness.[147,148] By using the above equation one can calculate the phase shift $\Delta\phi$ due to the change in optical path length. However, this semiquantitative analysis led to a 60% discrepancy between theoretical and experimental results. The author justified this discrepancy as a result of the variation of palladium properties, nonuniformity of the Pd thickness, etc. However, it ought to be remembered that this discrepancy may arise because for hydrogen concentration around 0.6% the β-phase transition becomes significant.

D. Comparison between purely electronic and optical fiber sensors

It appears that coherent light does seem to be very competitive with contemporary modern electronics as a hydrogen-sensing principle. The propagation of light waves is, however, very sensitive to the absorption, reflection, and transmission in the propagation medium. Nevertheless, the choice of wavelength-selective fibers has minimized and even made these problems negligible. The material for the optical waveguide is carefully chosen for selected wavelengths at which dispersion and attenuation in the fiber are minimal. In what follows we describe some of the attractive features and disadvantages of chemical sensors based on fiber optics. (i) The optical nature of the signal does not introduce any electrical interference. This advantage makes FOS very useful in environments with considerable electromagnetic activity. (ii) The most exciting possibility offered by chemical fiber optics appears to be [144] the use of multiwavelength and time-domain information. For example, one envisages sensors that report simultaneously the detection of two or more pollutants. Naturally, is it important to note that other detectors described in previous sections also share this advantage. However, for simultaneous detection of different gases the coated catalyst has an important and well-defined role to play. (iii) Optical sensors can be developed to respond in environments incompatible with electroded devices. (iv) Their small size makes optical fibers attractive for beam guidance to and from remote sensors.

Unfortunately, FOS are subject to several limitations as compared to electronic solid state devices. The most important is that the ambient light could interfere with background noise level. Thus FOS require a dark environment for optimal operation and noise minimization.

V. ELECTROCHEMICAL SENSORS

A. Introduction and historical perspective

As was pointed out in Sec. I A, the detection of hydrogen is very important for several reasons and especially in the chemical industry. For example, a need for a rugged device to determine hydrogen in the environment and hydrogen dissolved in metals led to the development of hydrogen electrochemical sensors.

The first electrochemical hydrogen sensor was developed by Childs *et al.*[156] in 1978. Since then, a limited number of solid-state electrochemical room-temperature hydrogen detectors have been developed as prototype cells,[157–160] and some of them have been applied to practical situations.[161–164] For example Hultquist[164] has used an electrochemical detector for the study of hydrogen evolution during the corrosion of copper in pure water. An electrochemical hydrogen sensor for use at elevated temperatures has been developed by Liaw *et al.*[165]

B. Theoretical background

As is well known any electrochemical cell is made up of an electrical conductive path involving two electrodes immersed in an ionic electrolyte. Each electrode exhibits its own characteristic potential. In recent years, solid state electrochemical cells of the type *gas permeable electrode/solid proton conducting electrolyte/gas permeable electrode,* have been developed as convenient devices for continuous measurements of flowing H_2. In such a geometry, H_2 provides the proton path, equivalent to electrolytic ionic conduction. The electron flux from the ionized protons manifests itself as a current in the external circuit, due to charge exchanges at the working electrode. Thus, the measured current is a monitor of the hydrogen/proton concentration in the electrochemical cell. One of the major advantages of these kinds of device is the fact that they follow a well-known mechanism (Nernst law)[166,167] and thus, they do not require calibration. According to Kumar and Fray the hydrogen sensor can

be described in terms of the following galvanic cell using the composite electrodes γ-MnO_2/HUP/acetylene black, and (α and β) PbO_2/HUP/acetylene black;[160] HUP stands for hydrogen uranyl phosphate electrolyte:

Metal/Test gas, Pt black/HUP/Reference electrode/Metal

Anode (A)	Cathode (C)

Cell: Reference electrode-(α and β) PbO_2/HUP.
Cell: Reference electrode-γ-MnO_2/HUP/Carbon black or graphite.

The potential difference (EMF) established between the working and the reference electrodes can be analyzed in terms of the following half-reactions:

Anode

$$H_2(\text{test gas}) \rightarrow 2H^+ \text{ (HUP)} + 2e^{-2}. \quad (57)$$

The above reaction takes place on an electrocatalytic surface such as Pt black, where the half-cell potential is related to the partial hydrogen pressure. The half-cell potential can be calculated from the Nerst expression given by the relation[166,167]

$$\Delta E = 2.303(RT/2F_a)\log P_{H_2} \quad (58)$$

where ΔE is the potential measured across the electrolyte, F_a is the Faraday ($= 10^4$ C/mole), R is the universal gas constant, and T is the absolute temperature. Pure H_2 at 1 atm pressure in equilibrium with HUP at a given temperature defines the standard half-potential, arbitrarily chosen as zero:

Cathode

$$\text{Cell I: } xPbO_2 + H^+ \text{ (HUP)} + e^- \rightarrow H(PbO_2)_x, \quad (59.1)$$

$$\text{Cell II: } xMnO_2 + H^+ \text{ (HUP)} + e^- \rightarrow H(MnO_2)_x. \quad (59.2)$$

The potential generated by these cells is due to the gradient of P_{H_2} between anode and cathode, and can also be given from Nernst's law:[166,167]

$$\Delta E_{\text{cell}} = 2.303 \frac{RT}{2F_a} \log \frac{P_{H_2}(\text{test gas})}{P^c_{H_2}}, \quad (60)$$

where $P^c_{H_2}$ represents the pressure of hydrogen in 1 atm.

C. Experiment and results

The method of preparation of the electrolyte hydrogen uranyl phosphate (HUP) has already been described by Lyon and Fray.[161] Figure 31 shows the setup of the HUP electrochemical detector.[160] The cell was constructed in the form of a sandwich where the middle layer of 1 mm thickness of HUP electrolyte lies between the thin reference electrode and the detector electrode, made of Pt black. According to Kumar and Fray[160] the electrical connection to the working electrode was made with the help of a stainless-steel mesh. The electrochemical measurements have been made by using a digital electrometer.

Figure 32 presents some experimental results obtained by Kumar and Fray.[160] This figure shows the variation of cell EMF as a function of the logarithm of P_{H_2} in the range of pure argon to 1% hydrogen in Ar. In Fig. 31 one can note the linear variation of EMF vs $\log(P_{H_2})$, with a slope of 28.9

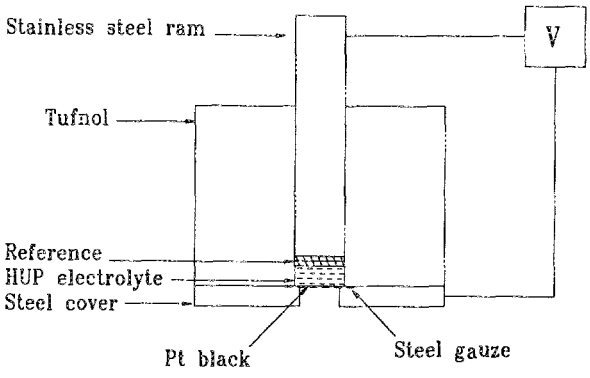

FIG. 31. Schematic diagram of the electrochemical hydrogen detector (from Ref. 160).

mV/decade at 17 °C, which is in excellent agreement with the value given by the Nernst Eq. (60). This result proves that it is possible to make excellent quantitative measurements down to 1% H_2 in Ar, using the linearity of the electrochemical sensor. The response times of this ionic sensor have been found to range from a few seconds (high pressures) to a few minutes (low pressures), a definite disadvantage over other faster solid-state electronic, molecular, and optical sensors.

According to Lungsgaard *et al.*[158] the electrochemical sensor has shown high durability and reproducibility: experimental results obtained by the electrochemical detector were reproduced with high fidelity at two-month intervals.

Before the end of this section we believe that it is important to include one more electrochemical device made by Miura *et al.*[168] This four-probe-type hydrogen sensor has been found to yield signals not only proportional to hydrogen concentration in air (see Fig. 33), but also independent of the relative humidity from 7%–90%. The response detection limit was found to be 2000 ppm in air at 25 °C.

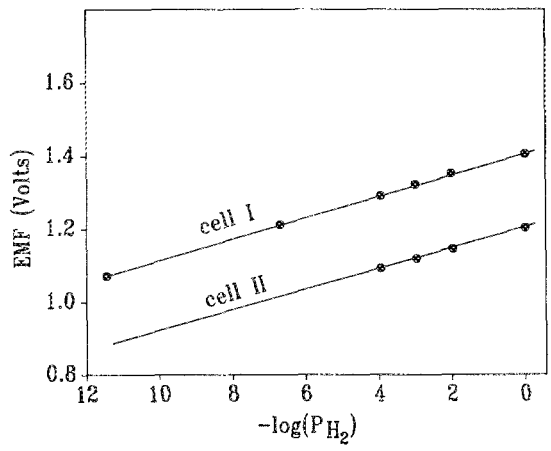

FIG. 32. Potential difference response as a function of the hydrogen partial pressure (from Ref. 160).

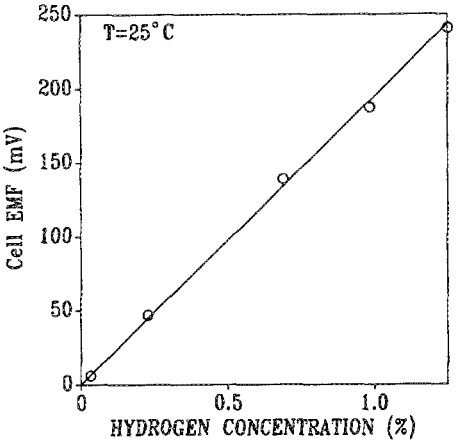

FIG. 33. Potential difference response as a function of the hydrogen concentration in air of the four-probe type electrochemical detector ($T = 25$ °C) (from Ref. 168).

VI. SEMICONDUCTOR HYDROGEN FLOW-THROUGH SENSORS

A. Introduction and historical perspective

The purpose of this section is to review briefly and in general terms the progress made in the field of chemical semiconductor hydrogen sensors. The reader is urged to consult the excellent paper by Lundström *et al.*[33] for detailed critical reviews of semiconductor hydrogen sensors. In this review attention is going to be given to semiconductor devices which have been used under flow-through conditions (in air or in inert atmosphere). Studies made under ultrahigh vacuum (UHV) conditions will be omitted. A list of pertinent devices will be given to point out the different characteristics and to discuss some features of their operating performances.

The development of the semiconductor technology has led to the emergence of semiconductor chemical sensors. The semiconductor chemical sensor is based on the metal oxide semiconductor (MOS) junction principle.[169] If a silicon single crystal is oxidized in oxygen or water vapor at high temperature, a high-quality silicon dioxide film is formed on the surface. MOS sensor devices can be made in two different ways (see Fig. 34): (a) as MOS capacitors and (b) as MOS transistors.[170]

As of 1966 a number of gas sensors based on hydrogen-induced changes in the electrical conductivity of MOS structures have been reported.[171-173] Furthermore, Lundström *et al.* developed a Pd-gate MOS transistor, and Pd-gate metal-insulator-semiconductor (MIS) sensors,[174,175] while Steele and MacIver showed that a Pd-CdS Schottky barrier diode exhibited a response to hydrogen.[176] The double metal-gate MIS Field Effect Transistor (FET) has also been used as a hydrogen sensor,[177] and so have been the insulated-gate field-effect transistor (IGFET),[174,178] and the hydrogen sensitive MOSFETs with a catalytic gate metal, such as Pd.[174] The first MOSFET device for hydrogen detection was described by Lundström *et al.*[174] in 1975. Since then more than one hundred papers have been published on the subject

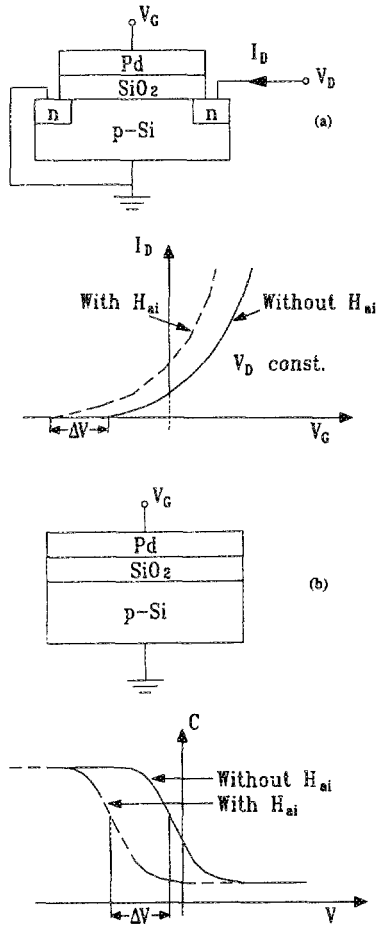

FIG. 34. Cross-sectional view and current-voltage characteristics of Pd-MOS (a) transistor, and (b) capacitor; *D*: drain; *G*: gate; H_{ai} hydrogen concentration at the Pd-oxide interface (from Refs. 10, 33, 170, and 191).

and many of them are given in Refs. 179–194. A number of review papers have already appeared.[33,170,195-201] The authors believe that it is important to indicate that Lundström's group in Sweden has played a leading role in the development of semiconductor sensors. According to Lundström,[10] when the device is exposed to hydrogen, dissociated hydrogen atoms absorbed at the Pd-SiO_2 interface are polarized and give rise to a dipole layer. This corresponds to a voltage drop, ΔV, which is added to the externally applied gate voltage V_G. The characteristics of the MOS hydrogen sensor consist of this voltage shift by ΔV. Typical voltage shifts from a Pd-MOS transistor and of Pd-MOS capacitor are shown in Figs. 34(a) and 34(b) as $I_D(V_G)$ and $C(V)$ curves, respectively.

B. Theoretical background and some experimental results

Several workers hypothesized that hydrogen molecules and atoms adsorbed on a metal surface act as dipoles and they give rise to macroscopic measurable voltage drop, or change in surface potential.[10] The dipole layer shifts the energy levels at the metal-insulator interface. We can distinguish four general device groups based on this principle: (i)

TABLE VI. A global comparison of solid-state hydrogen sensors under flow-through conditions. ?:No data available/reported.

Refs.	Type	Year	L (A)	T (°C)	Carrier gas	Sensitivity
24	Pd-$LiTaO_3$	1981	3000?	20	N_2	1%
26-30	Pd-PPE	1989	130	20	N_2	40 ppm
62,63	Pd-PQCMB	1989	800	20	N_2	0.5%
76	Pd-PQCMB	1976	?	81	N_2	350 ppm
120	Pd-SAW	1982	3000	20	N_2	50 ppm
147	Pd-FOS	1984	?	20	N_2	0.2%
148	Pd-FOS	1988	15000	20	N_2	20 ppb
160	Pd-HUP	1988	···	20	?	100 ppm
168	Four-probes	1987	···	25	air	2000 ppm
180	Pd-MOS	1975	100	150	air	40 ppm
174	Pd-MOS	1975	10	100	air	10 ppm
182	Pd-MOS	1982	?	150	air	1 ppm
182	Pd-MOS	1982	?	150	N_2	0.03 ppb
179	Pd-MIS	1983	350	22	N_2	100 ppm
176	Pd-diode	1976	800	25	N_2	100 ppm
181	Pd-MOS	1981	?	150	O_2	10-100 ppm

MOS-transistor, (ii) MOS-capacitor, (iii) MIS-capacitor, and (iv) Schottky barrier. The characteristics of several of these kinds of devices, among others, are presented in Table VI. Figure 35 shows a typical experimental setup for measuring the hydrogen sensitivity of the Pd-gate-MOS transistor.[170] The voltage is recorded as a function of time for various hydrogen concentrations. Figure 36 shows time-dependent responses from this device. The response time was found to be 10 s. Figures 37(a) and 37(b) show the variation of the saturated voltage ΔV_s as a function of hydrogen concentration at 210 and 240 [Fig. 37(a)], and 150 °C [Fig. 37(b)]. The solid lines in this figure show a fit to the Langmuirian isotherm,[10] similar to the one advanced for the photopyroelectric sensor:

$$\Delta V_s = \Delta V_{\max}\left(\frac{K(T)\sqrt{P_{H_2}}}{1+K(T)\sqrt{P_{H_2}}}\right), \tag{61}$$

where $\Delta V_{\max}$ is the maximum voltage output of the device [$\Delta V = 0.5$ V in Fig. 37(a)].

VII. GENERAL DISCUSSION, COMPARISONS, AND CONCLUDING REMARKS

Table VI contains a global comparison of characteristic parameters of several hydrogen detectors, which have been presented in this review. In this table information is presented on the year of development of each type of detector, the thickness of the Pd layer (L) coated on the device, the operating temperature, the carrier gas under which the experiments were performed, and finally the sensor sensitivity limit. The response time of the detectors has not been reported on the table because (i) many authors have defined the response time in a different way; (ii) this time depends on the volume of the test cell,[83] and (iii) it also depends on the flow rate. The main points of this Table and of this review can be summarized as follows:

(1) All H_2 sensors (presented in this paper) use a Pd metal trap, except for the four-probe electrochemical device.

(2) The oxidation of the palladium layer introduces significant problems for the operation of the hydrogen detectors.[33,62,63]

(3) The MOSFET hydrogen sensors have the longest history of research and development. This is one of the reasons why much more knowledge concerning their operating mechanism has been accumulated than for other sensors.

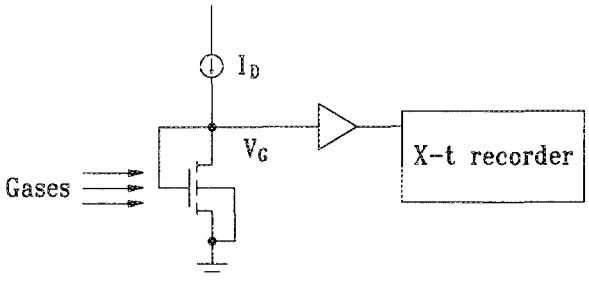

FIG. 35. Electronic setup of the Pd-gate MOS sensor transistor (from Ref. 170).

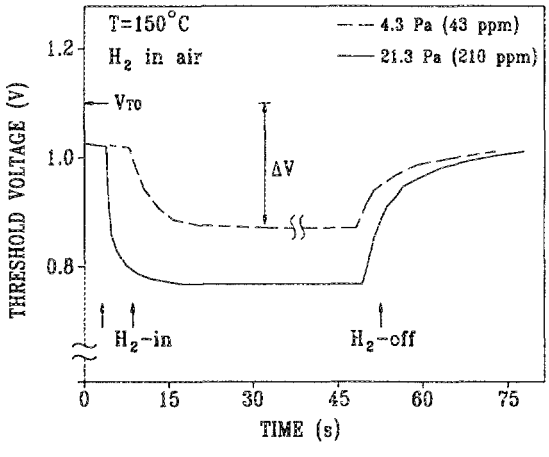

FIG. 36. Pd-gate MOS transistor responses as a function of time, for two concentrations (43 and 210 ppm) of hydrogen in air ($T = 150$ °C) (from Refs. 10 and 170).

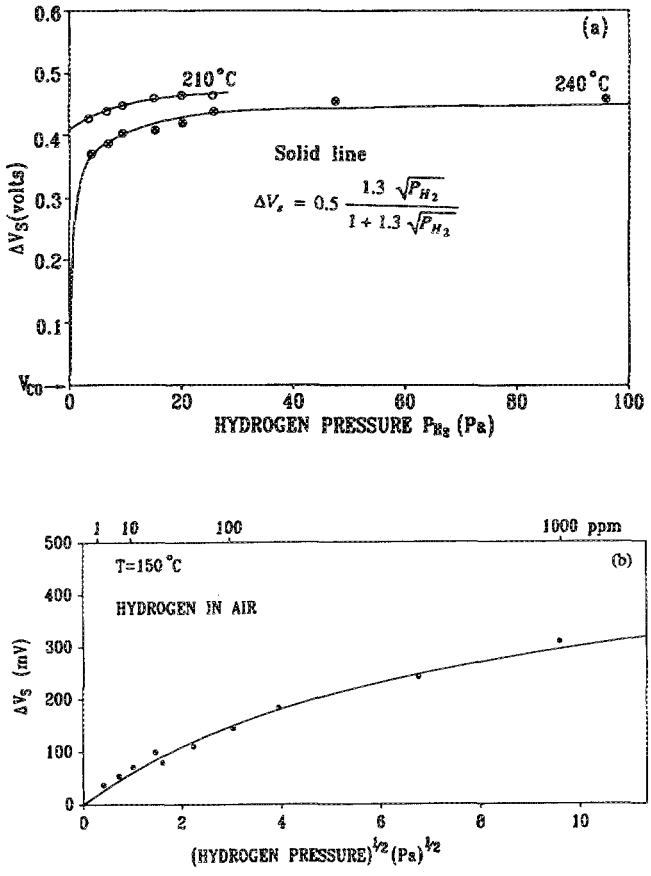

FIG. 37. Variation of the threshold saturated voltage ΔV_s as a function of the square root of the hydrogen pressure. Solid lines: Langmuirian isotherm fit to the data, as per Eq. (61). (a) at 210 –O– and 240 °C –●– and (b) at 15 °C (from Refs. 10 and 170).

(4) MOSFET devices usually operate under high temperature; otherwise their sensitivity and response time are adversely affected.[33] On the other hand, the non-FET devices usually operate under room-temperature conditions.

(5) At high temperature the FET devices present sensitivities at least three orders of magnitude greater than the best non-FET sensor.

(6) At room temperature, the highest sensitivity has been exhibited by the Pd-FOS device. We note the enormous progress that has been achieved by the Pd-FOS device. In four years the all-optical sensor became more than 8 orders of magnitude more sensitive than the first generation device. Thus, the Pd-FOS is actually the most sensitive detector in the entire group of solid-state H_2 sensing devices at room temperature.

(7) We note that the photopyroelectric sensor is the second best in terms of sensitivity in the group of non-FET devices even though it has only been developed very recently. The ac photopyroelectric device has been found to be almost three orders of magnitude more sensitive than the dc-pyroelectric sensor.

(8) Operation at 80.3 °C of the piezoelectric crystal microbalance leads to a sensitivity 15 times better than that at room temperature. Operation at low H_2 concentrations is impeded by interference from other ambient gases.

(9) The SAW piezoelectric device is much more sensitive than the bulk piezoelectric sensor.

(10) The Pd-HUP electrochemical sensors have relatively low sensitivity compared with the other FET and non-FET devices.

(11) The MOSFET devices have a good sensitivity even when the carrier gas is not inert. For example, the Pd-MOS device is able to detect up to 10 ppm, even when the carrier gas is oxygen.[181]

ACKNOWLEDGMENTS

The authors wish to acknowledge the support of the Ministry of Energy, Mines, and Resources Canada (EMR) toward the development of the Pd photopyroelectric and of the flow-through Pd-PQCMB hydrogen sensors, through a contract to CHES. Financial support of EMR for this work is also gratefully acknowledged. The assistance in figure drawing by Kamyar Ghandi has been valuable toward the preparation of the final form of this manuscript.

Note added in proof. It has come to the attention of the present authors that a new ac dielectric device has been fabricated as a flow-through hydrogen sensor.[202] This new device utilizes optical excitation and electrical detection techniques similar to ones presented for the ac photopyroelectric sensor in this Review.[27] It consists of a Pd film-mica-Au capacitor. Preliminary experimental results are consistent with the thermal modulation of the contact potential difference between the Pd and the Au counter-electrode and a reference structure involving a metal electrode inert to hydrogen as the proposed operating mechanism for this new sensor.

[1] E. F. P. Vaz de Campos, Int. J. Hydrogen Energy **12**, 847 (1987).
[2] R. M. Dell, in *Solid-State Protonic Conductors for Fuel Cells and Sensors; Part II*, edited by J. B. Goodenough, J. Jensen, and M. Kleitz (Odense University Press, Odense, 1982), p. 13.
[3] W. Peschka, Int. J. Hydrogen Energy **12**, 753 (1987).
[4] R. C. Weast, in *Handbook of Chemistry and Physics* (CRC, Cleveland, 1976), p. D-107.
[5] W. H. Kings, Environ. Sci. Technol. **4**, 1136 (1970).
[6] F. A. Lewis, *The Palladium Hydrogen System* (Academic, New York, 1967).
[7] M. Armgarth, D. Söderbrerg, and I. Lundström, Appl. Phys. Lett. **41**, 654 (1982).
[8] G. A. Somorjai, *Principles of Surface Chemistry* (Prentice-Hall, Englewood Cliffs, 1972), Chap. 5.
[9] J. M. Thomas and W. J. Thomas, *Introduction to the Principles of Heterogeneous Catalysis* (Academic, New York, 1967), Chap. 2.
[10] K. I. Lundström, Sensors and Actuators **1**, 403 (1981).
[11] G. J. Macly, IEEE Trans. Electron Dev. **ED-32**, 1158 (1985).
[12] H. Conrad, G. Ertl, and E. E. Latta, Surf. Sci. **41**, 435 (1974).
[13] F. Daniels and R. A. Alberty, in *Physical Chemistry*, 2nd ed. (Wiley, New York, 1961).
[14] W. C. Roentgen, Ann. Phys. **45**, 737 (1914).
[15] S. B. Lang, *Temperature: Its measurement and control in Science and Industry*, edited by C. M. Herzfeld (Reinhold, New York, 1962), Vol. 3, p. 1015.
[16] H. Rahnamai and J. N. Zemel, Sensors and Actuators **2**, 3 (1981/82).
[17] H. Rahnamai and J. N. Zemel, Sensors and Actuators **3**, 203 (1983).
[18] H. Rahnamai, Sensors and Actuators **3**, 17 (1982).
[19] J. R. Frederick, J. N. Zemel, and N. Goldfine, J. Appl. Phys. **57**, 4936 (1985).
[20] A. Hadni, in *Infrared and Millimeter Waves* (Academic, New York, 1980), Vol. 3, Chap. 3.
[21] M. Okuyama, Y. Togami, Y. Hamakawa, M. Kimata, and S. Uematsu, Sensors and Actuators **16**, 263 (1989).

[22] J. N. Zemel, B. Keramati, C. W. Spivak, and A. D'Amico, Sensors and Actuators **1**, 427 (1981).
[23] A. D'Amico, G. Fortunato, W. Reihua, and J. N. Zemel, *IEEE International Conference on Solid State Sensors and Actuators* (Transducers '85, New York, 1985), p. 239.
[24] J. N. Zemel, in *Solid State Chemical Sensors*, edited by J. Janata and R. J. Huber (Academic, New York, 1985), Chap. 4.
[25] A. D'Amico and J. N. Zemel, J. Appl. Phys. **57**, 2460 (1985).
[26] A. Mandelis and C. Christofides, Sensors and Actuators **2**, 77 (1990).
[27] C. Christofides and A. Mandelis, J. Appl. Phys. **66**, 3975 (1989).
[28] C. Christofides and A. Mandelis, in *Proceedings of the 1989 IEEE Ultrasonic Symposium* (Montreal, 1989) (in press).
[29] A. Mandelis and C. Christofides J. Vac. Sci. Technol. A (in press).
[30] A. Mandelis and C. Christofides, *6th International Topical Meeting on Photoacoustic and Photothermal Phenomena II, Baltimore, MD, USA, July 31–Aug. 3* (1989) Springer Series in Optical Sciences Vol. 62, pp. 347–350 (1989).
[31] Operating and Service Manual, EG&G PRINCETON APPLIED RESEARCH, Model 5204 (Lock-in Analyzer); "Ratio Option," pp. 23 and 24.
[32] KYNAR Piezo Film Technical Manual, Pennwalt Corp., King of Prussia, PA (1983).
[33] K. I. Lundström, M. Armgarth, L-G. Petersson, CRC Critical Reviews in Solid State and Material Sciences **15**, 201 (1989).
[34] M. Armgarth and C. Nylander, IEEE Electron Device Lett. **EDL-3**, 384 (1982).
[35] A. D'Amico, A. Palma, and E. Verona, in *Proceedings of the 1982 IEEE Ultrasonics Symposium* (San Diego, 1982), p. 308.
[36] R. Lalauze, Ph. Gillard, and C. Pijolat, Sensors and Actuators **14**, 243 (1988).
[37] S. Qian and D. O. Northwood, Int. J. Hydrogen Energy **13**, 25 (1988).
[38] W. H. King, Anal. Chem. **36**, 1735 (1964).
[39] W. H. King, U. S. Patent No. 3 164 004 (Jan. 5, 1965). **4**, 1136 (1970).
[40] W. H. King, Res. Dev. **20**, 28 (1969).
[41] W. H. King, *Vacuum Microbalance Techniques*, edited by A. W. Czanderna (Plenum, New York, 1981), Vol. 8, p. 183.
[42] G. Z. Sauerbrey, Z. Phys. **155**, 206 (1959).
[43] G. Z. Sauerbrey, Z. Phys. **178**, 457 (1964).
[44] A. L-Roman and G. G. Guilbault, Anal. Lett. **5**, 225 (1972).
[45] M. W. Frechette and J. L. Fasching, Environ. Sci. Technol. **7**, 1135 (1973).
[46] F. W. Karasek and J. M. Tiernay, J. Chromatogr. **89**, 31 (1974).
[47] J. L. Cheney and J. G. Homolya, Anal. Lett. **8**, 175 (1975).
[48] K. H. Karmarkar, L. M. Webber, and G. G. Guilbault, Anal. Chim. Acta **81**, 265 (1976).
[49] K. H. Karmarkar and G. G. Guilbault, Anal. Chim. Acta **75**, 111 (1975).
[50] J. Hlavay and G. G. Guilbault, Anal. Chem. **50**, 965 (1978).
[51] W. M. Shackleford and G. G. Guilbault, Anal. Chim. Acta **73**, 383 (1974).
[52] E. P. Scheide and G. G. Guilbault, Anal. Chem. **44**, 1764 (1972).
[53] G. G. Guilbault and Y. Tomita, Sensors and Actuators **2**, 43 (1981/82).
[54] Y. Tomita, M. H. Ho, and G. G. Guilbault, Anal. Chem. **51**, 1475 (1979).
[55] M. Janghorbani and H. Freund, Anal. Chem. **45**, 325 (1973).
[56] G. G. Guilbault, Anal. Chim. Acta **39**, 260 (1967).
[57] M. R. Deakin and H. Byrd, Anal. Chem. **61**, 290 (1989).
[58] J. P. Randin and F. Zulling, Sensors and Actuators **11**, 319 (1987).
[59] C. W. Lee, Y. S. Fung, and K. W. Fung, Anal. Chem. Acta **135**, 277 (1982).
[60] M. Christen, Sensors and Actuators **4**, 555 (1983).
[61] S. Abe and T. Hosoya, in *Proceedings of the 5th World Hydrogen Energy Conference*, 1893 (Pergamon, New York, 1984), Vol. 4.
[62] C. Christofides and A. Mandelis, J. Appl. Phys. **66**, 3986 (1989).
[63] C. Christofides and A. Mandelis, *CSME Annual Meeting* (Toronto, 1990) Vol. I, pp. 467–470.
[64] A. Kindlund and I. Lundström, Sensors and Actuators **3**, 63 (1982/83).
[65] G. J. Bastiaans, in *Chemical Sensors*, edited by T. E. Edmonds (Chapman and Hall, New York, 1988), Chap. 14.
[66] J. R. Lasher, Proc. Roy. Soc. (London) A **161**, 525 (1937).
[67] D. H. Everett and P. Nordon, Proc. R. Soc. (London) A **259**, 341 (1960).
[68] J. W. Simons and T. B. Flanagan, Can. J. Chem. **43**, 1665 (1965).
[69] J. W. Simons and T. B. Flanagan, J. Phys. Chem. **69**, 3773 (1965).
[70] R. J. Behm, K. Christmann, and G. Ertl, Surf. Sci. **99**, 320 (1980).
[71] V. Ponec, Z. Knor, and S. Cerny, Discuss. Faraday Soc. **41**, 149 (1969).
[72] J. Llopis, J. Catal. Rev. **2**, 161 (1968).
[73] M. A. Vannice, J. E. Benson, and M. Boudart, J. Catal. **16**, 348 (1970).
[74] P. A. Sermon, J. Catal. **24**, 460 (1972).
[75] G. A. Frazier and R. Glosser, J. Phys. D **12**, L113 (1979).
[76] R. V. Bucur, V. Mecea, and T. B. Flanagan, Surf. Sci. **54**, 477 (1976).
[77] R. V. Bucur, V. Mecea, and E. I. Indrea, J. Less-Common Metals **49**, 147 (1976).
[78] R. V. Bucur, J. Catal. **70**, 92 (1981).
[79] B. Kasemo and E. Tornquist, Phys. Rev. Lett. **44**, 1555 (1980).
[80] V. Mecea and R. V. Bucur, J. Vac. Sci. Technol. **17**, 182 (1980).
[81] G. A. Frazier and R. Glosser, J. Less-Common Metals **74**, 89 (1980).
[82] M. C. Steele, J. W. Hile, and B. A. MacIver, J. Appl. Phys. **47**, 2537 (1986).
[83] J. B. Cooper, J. H. Edmondson, D. M. Joseph, and R. S. Newbower, IEEE Trans. Biomed. Eng. **BME-28**, 459 (1981).
[84] J. B. Cooper, R. S. Newbower, D. A. Sebok, and T. K. Meng, in *Proceedings of the 32nd ACEMB* (Alliance for Engineering in Medicine and Biology, Denver, 1979). Vol. 21, p. 15.
[85] Lord Rayleigh, London Math. Soc. Proc. **17**, 4 (1885).
[86] R. M. White and F. W. Voltmer, Appl. Phys. Lett. **7**, 314 (1965).
[87] D. Hauden, G. Jaillet, and R. Coquerel, in *Proceedings of the 1981 IEEE Ultrasonics Symposium* (IEEE, Chicago, 1981), p. 148.
[88] D. Hauden, M. Planat, and J. J. Gagnepain, IEEE Trans. Sonics Ultrason. **SU-28**, 342 (1981).
[89] D. E. Cullen and T. M. Reeder, in *Proceedings of the 1975 IEEE Ultrasonics Symposium* edited by J. de Klerk (IEEE, Los Angeles), p. 519.
[90] E. J. Staples, J. Wise, and R. E. DeWames, in *Proceedings of the 1981 IEEE Ultrasonics Symposium* (IEEE, Chicago, 1981), p. 155.
[91] D. E. Cullen and G. K. Montress, in *Proceedings of the 1980 IEEE Ultrasonics Symposium* (IEEE, Boston, 1980), p. 696.
[92] K. Toda and K. Mizutani, J. Acoust. Soc. Am. **74**, 667 (1983).
[93] S. G. Joshi, Rev. Sci. Instrum. **54**, 1012 (1983).
[94] R. Inaba, Y. Kasahara, and K. Wasa, in *Proceedings of the 1982 IEEE Ultrasonics Symposium* (IEEE, San Diego, 1982), p. 312.
[95] E. Gatti, A. Palma, and E. Verona, Sensors and Actuators **4**, 45 (1983).
[96] E. Gatti, A. Palma, and E. Verona, *Proceedings of the 1983 IEEE Ultrasonics Symposium* (IEEE, Atlanta, 1983), p. 291.
[97] A. Palma, L. Palmieri, G. Sociono, and E. Verona, in *Proceedings of the 1984 IEEE Ultrasonics Symposium* (IEEE, Dallas, 1984), p. 951.
[98] S. W. Hanna, IEEE Trans. Ultrasonics, Ferroelectrics Freq. Control **UFFC-2**, 191 (1987).
[99] H. F. Tiersten, D. S. Stevens, and P. K. Das, in *Proceedings of the 1980 IEEE Ultrasonics Symposium* (IEEE, Boston, 1980), p. 692.
[100] P. Artemann and P. L. Meunier, in *Proceedings of the 1981 IEEE Ultrasonics Symposium* (IEEE, Chicago, 1981), p. 152.
[101] P. L. Meunier and P. Hartemann, in *Proceedings of the 1982 IEEE Ultrasonics Symposium* (IEEE, San Diego, 1982), p. 299.
[102] P. Hartemann and P. L. Meunier, in *Proceedings of the 1983 IEEE Ultrasonics Symposium* (IEEE, Atlanta, 1983), p. 291.
[103] D. Hauden, F. Bindler, and R. Coquerel, in *Proceedings of the 1985 IEEE Ultrasonics Symposium* (IEEE, San Francisco, 1985), p. 486.
[104] D. Hauden and B. Loewenguth, Appl. Phys. Lett. **47**, 1271 (1985).
[105] M. Ishido, T. Imaizumi, and M. Toyoda, IEEE Trans. Instrum. Meas. **IM-36**, 83 (1987).
[106] N. Ahmad, in *Proceedings of the 1985 IEEE Ultrasonics Symposium* (IEEE, San Francisco, 1985), p. 483.
[107] B. Y. Lao, in *Proceedings of the 1980 IEEE Ultrasonics Symposium* (IEEE, Boston, 1980), p. 687.
[108] H. Wohltjen and R. E. Dessy, Anal. Chem. **51**, 1458 (1979).
[109] E. T. Zellers, R. M. White, S. M. Rappaport, and S. W. Wenzel, in *Proceedings of the 1987 IEEE Ultrasonics Symposium* (IEEE, Denver, 1987), p. 459.
[110] C. T. Chuang, and R. M. White, in *Proceedings of the 1981 IEEE Ultrasonics Symposium* (IEEE, Chicago, 1981), p. 159.
[111] H. W. Wohltjen, A. W. Snow, W. R. Barger, and D. S. Ballantine, IEEE Trans. Ultrasonics, Ferroelectrics Freq. Contr. **UFFC-34**, 172 (1987).
[112] S. J. Martin, A. J. Ricco, D. S. Ginley, and T. E. Zippereian, IEEE Trans. Ultrasonics, Ferroelectrics, Frequency Contr. **UFFC-34**, 143 (1987).
[113] A. Bryant, D. L. Lee, and J. F. Vitelino, in *Proceedings of the 1981 IEEE Ultrasonics Symposium* (IEEE, Chicago, 1981), p. 171.
[114] A. D'Amico, A. Petri, P. Verardi, and E. Verona, in *Proceedings of the 1987 IEEEUltrasonics Symposium* (IEEE, Denver, 1987), p. 633.
[115] S. G. Joshi and J. G. Brace, in *Proceedings of the 1985 IEEE Ultrasonics Symposium* (IEEE, San Francisco, 1985), p. 600.

[116] J. G. Brace, T. S. Sanfelippo, and S. G. Joshi, Sensors and Actuators **14**, 47 (1988).
[117] A. Bryant, M. Poirier, G. Riley, D. L. Lee, and J. F. Vitelino, Sensors and Actuators **4**, 105 (1983).
[118] A. D'Amico and E. Verona, Sensors and Actuators **17**, 55 (1989).
[119] A. D'Amico, A. Palma, and E. Verona, Appl. Phys. Lett. **41**, 300 (1982).
[120] A. D'Amico, A. Palma, and E. Verona, Sensors and Actuators **3**, 31 (1982/83).
[121] A. D. Amico, M. Gentili, P. Verardi, and E. Verona, in *Proceedings of the 2nd International Meeting on Chemical Sensors* (Bordeaux, 1986), p. 743.
[122] H. Wohltjen, Sensors and Actuators **5**, 307 (1984).
[123] H. Wohltjen, A. Snow, and D. Ballantine, in *Proceedings of the 1985 IEEE Ultrasonics Symposium* (IEEE, San Francisco, 1985), p. 66.
[124] B. A. Auld, *Acoustic Fields and Waves in Solids* (Wiley-Interscience, New York, 1973), Vol. 2, Chap. 12.
[125] D. S. Ballantine, S. L. Rose, J. W. Grate, and H. Wohltjen, Anal. Chem. **58**, 3058 (1986).
[126] A. J. Ricco, S. J. Martin, and T. E. Zipperian, Sensors and Actuators **8**, 319 (1985).
[127] J. Dakin and B. Culshaw, in *Optical Fiber Sensors: principles and components* (Artech House, Boston, 1988).
[128] B. G. Gamble, P. G. Hugenholtz, R. G. Monroe, M. Polanyi, and A. S. Nadas, I. Intracardiac Oximetry Circulation (1965), Vol. 31, p. 328.
[129] E. Kotte, K. Derge, R. R. Landeryou, P. Propawe, T. Tschudi, and W. Wobbe, *Technologies of Light* (Springer, Berlin, 1989), Chap. 4.
[130] G. B. Hocker, Appl. Opt. **18**, 1445 (1979).
[131] R. Hughes and J. Jarzynski, Appl. Opt. **19**, 98 (1980).
[132] D. H. Leslie, G. L. Trusty, A. Dandridge, and T. G. Giallorenzi, Electron. Lett. **17**, 581 (1981).
[133] A. Yariv and H. V. Winsor, Opt. Lett. **5**, 87 (1980).
[134] J. Jarzynski, J. H. Cole, J. A. Bucaro, and C. M. Davis, Appl. Opt. **19**, 3746 (1980).
[135] J. I. Peterson, S. R. Goldstein, and R. V. Fitzgerald, Anal. Chem. **52**, 864 (1980).
[136] E. Smela and J. J. S-Aviles, Sensors and Actuators **13**, 117 (1988).
[137] J. I. Peterson and G. G. Vurek, Science **244**, 123 (1984).
[138] E. E. Hardy, D. J. David, N. S. Kapany, F. C. Unfortunately, Nature **257**, 666 (1975).
[139] D. J. David, M. C. Willson, and D. S. Ruffin, Anal. Lett. **9**, 389 (1976).
[140] J. F. Giuliani, H. Wohltjen, and N. L. Jarvis, Opt. Lett. **8**, 54 (1983).
[141] J. F. Giuliani, P. P. Bey, Jr., H. Wohltjen, A. Snow, and N. L. Jarvis, *IEEE International Conference on Solid-State Sensors and Actuators* (IEEE, New York, 1985), p. 74.
[142] A. L. Harmer and R. Narayanaswamy, in *Chemical Sensors*, edited by T. E. Edmonds (Chapman and Hall, New York, 1988), Chap. 13.
[143] C. Nylander, J. Phys. E. Sci. Instrum. **18**, 736 (1985).
[144] W. R. Seitz, Anal.Chem. **56**, 16A (1984).
[145] I. Chabay, Opt. Waveguides Anal. Chem. **54**, 1071A (1982).
[146] A. L. Harmer, *Proceedings of the Symposium on Chemical Sensors*, edited by D. R. Turner (Electrochemical Society, Honolulu, 1987), Vol. 87–9, p. 409.
[147] M. A. Butler, Appl. Phys. Lett. **45**, 1007 (1984).
[148] M. A. Butler and D. S. Ginley, J. Appl. Phys. **64**, 3706 (1988).
[149] B. W. Prahl and P. M. Tracey, Sensors (**August**), 48 (1986).
[150] J. P. Laude, J. Flamand, J. C. Gautherin, D. Lepere, P. Gacoin, F. Bos, and J. Lerner, *European Conference on Optical Communications*, Geneva, Switzerland, 1983 (North-Holland, Amsterdam, 1983), p. 417.
[151] H. E. Korth, J. Phys. (Paris) **44**, C10, 101 (1983).
[152] H. E. Korth, *Second International Conference on Optical Fiber Sensors* (VDE-Verlag, Stuttgart, 1984), p. 219.
[153] P. K. Tien and R. J. Capik, *Topical Meeting on Integrated and Guided-wave Optics* (Nevada, 1980), p. TuB3-1.
[154] P. Kubelka and F. Munk, Z. Techn. Physik **12**, 593 (1931).
[155] M. A. Butler and D. S. Ginley, J. Electrochem. Soc. **135**, 45 (1988).
[156] P. E. Childs, A. T. Howe, and M. G. Shilton, J. Power Sources **3**, 105 (1978).
[157] A. T. Howe, S. H. Sheffield, P. E. Childs, and M. G. Shilton, Thin Solid Films **67**, 365 (1980).
[158] J. S. Lundsgaard, J. Malling, and M. L. Birchall, Solid State Ionics **7**, 53 (1982).
[159] J. Schoonman, D. R. Franceschetti, and J. W. Hanneken, Ber. Bunsenges. Phys. Chem. **86**, 701 (1982).
[160] R. V. Kumar and D. J. Fray, Sensors and Actuators **15**, 185 (1988).
[161] S. B. Lyon and D. J. Fray, Solid State Ionics **9-10**, 1295 (1983).
[162] K. A. Eagles and D. J. Fray, in *Proceedings of the Conference U. K. Corrosion 1984* (Inst. Corrosion Sc. Technol., Birmingham, 1984), p. 199.
[163] S. B. Lyon and D. J. Fray, Brit. Corros. J. **19**, 23 (1984).
[164] G. Hultquist, Corrosion Sci. **26**, 173 (1986).
[165] B. Y. Liaw, G. Deublein, and R. A. Huggins, in *Proceedings of the Symposium on Chemical Sensors*, edited by D. R. Turner, (Electrochemical Society, Honolulu, 1987), Vol. 87–9, p. 91.
[166] M. J. Sienko and R. A. Plane, Chemistry: Principle and Properties (McGraw-Hill, New York, 1966), p. 304.
[167] D. H. Busch, H. Schull, and R. T. Conley, *Chemistry* 2nd edition (Allyn and Bacon Inc., Boston. 1978), Chap. 17.
[168] N. Miura, T. Harada, and N. Yamazoe, in *Proceedings of the Symposium on Chemical Sensors*, edited by D. R. Turner, (Honolulu, 1987), Vol. 87–9, p. 163.
[169] S. M. Sze, *Physics of Semiconductors Devices* (Wiley-Interscience, London, 1969).
[170] I. N. Lundström, and C. Svensson, in *Solid State Chemical Sensors*, edited by J. Janata and R. J. Huber (Academic, New York, 1985), Chap. 1.
[171] T. Seiyama and S. Kagawa, Anal. Chem. **38**, 1069 (1966).
[172] P. J. Shaver, Appl. Phys. Lett. **11**, 255 (1967).
[173] H. Obayashi, Y. Sakurai, and T. Gejo, J. Solid State Chem. **17**, 299 (1976).
[174] K. I. Lundström, M. S. Shivaraman, and C. M. Svensson, J. Appl, Phys. **46**, 3876 (1975).
[175] K. I. Lundström, M. S. Shivaraman, and C. M. Svensson, Surf. Sci. **64**, 497 (1977).
[176] M. C. Steele and B. A. MacIver, Appl. Phys. Lett. **28**, 687 (1976).
[177] T. Yamamoto and M. Morimoto, Appl. Phys. Lett. **20**, 269 (1972).
[178] T. L. Poteat and B. Lalevic, IEEE Trans. Electron Dev. **ED-29**, 123 (1982).
[179] A. D'Amico, G. Fortunato, G. Petrocco, and C. Culuzza, Sensors and Actuators **4**, 349 (1983).
[180] I. Lundström, S. Shivaraman, C. Svensson, and L. Lundkvist, Appl. Phys. Lett. **26**, 55 (1975).
[181] M. Armgarth and C. Nylander, Appl. Phys. Lett. **39**, 91 (1981).
[182] M. Armgarth, C. Nylander, H. Sundgren, and I. Lundström, *Proceedings of the 4th World Hydrogen Energy Conference* (Pergamon, Pasadena, 1982), Vol. 4, p. 1717.
[183] S. Y. Choi, K. Takahashi, and T. Matsuo, IEEE Elect. Device Lett. **EDL-5**, 14 (1984).
[184] G. Fortunato, A. Bearzotti, C. Caliendo, and A. D'Amico, Sensors and Actuators **16**, 43 (1989).
[185] N. J. Evans, M. C. Petty, and G. G. Roberts, Sensors and Actuators **9**, 165 (1986).
[186] G. Fortunato, A. D'Amico, C. Coluzza, F. Sette, C. Capasso, F. Patella, C. Quaresima, and P. Perfetti, Appl. Phys. Lett. **44**, 887 (1984).
[187] S. J. Fonash, H. Huston, and S. Ashok, Sensors and Actuators **2**, 363 (1982).
[188] K. I. Lundström and D. Söderberg, Sensors and Actuators **2**, 105 (1981/82).
[189] K. I. Lundström, M. S. Shivaraman, and C. M. Svensson, Surf. Sci. **64**, 497 (1977).
[190] N. J. Evans, G. G. Roberts, and M. C. Petty, Sensors and Actuators **16**, 255 (1989).
[191] K. I. Lundström, Sensors and Actuators **2**, 105 (1981/82).
[192] M. Ogita, D. B. Ye, K. Kawamura, and T. Yamamoto, Sensors and Actuators **9**, 157 (1986).
[193] T. L. Poteat and B. Lalevic, IEEE Electron. Devices Lett. **EDL-2**, 82 (1981).
[194] W. Reihua, G. Fortunato, and A. D'Amico, Sensors and Actuators, **7**, 253 (1985).
[195] P. Bergveld and N. F. de Rooij, Sensors and Actuators **1**, 5 (1981).
[196] J. N. Zemel, Sensors and Actuators **1**, 31 (1981).
[197] S. R. Morrison, Sensors and Actuators **2**, 329 (1982).
[198] P. Bergveld, Sensors and Actuators **8**, 109 (1985).
[199] A. A. Saanan and P. Bergveld, Sensors and Actuators **7**, 75 (1985).
[200] I. N. Lundström, M. Armgarth, A. Spetz, and F. Winguist, Sensors and Actuators **10**, 399 (1986).
[201] I. Robins, in *Chemical Sensors*, edited by T. E. Edmonds (Chapman and Hall, New York, 1988), Chap. 10.
[202] A. Balasubramanian, J. J. Santiago-Aviles, and J. N. Zemel (unpublished)